

Energy, economy, and emissions: A non-linear state space approach to projections

Mikkel Bennedsen* Eric Hillebrand* and Jingying Zhou Lykke*

March 8, 2024

Abstract

We propose a non-linear state-space model to examine the relationship between CO₂ emissions, energy sources, and macroeconomic activity, using data from 1971 to 2019. CO₂ emissions are modeled as a weighted sum of fossil fuel use, with emission conversion factors that evolve over time to reflect technological changes. GDP is expressed as the outcome of linearly increasing energy efficiency and total energy consumption. The model is estimated using CO₂ data from the Global Carbon Budget, GDP statistics from the World Bank, and energy data from the International Energy Agency (IEA). Projections for CO₂ emissions and GDP from 2020 to 2100 from the model are based on energy scenarios from the Shared Socioeconomic Pathways (SSP) and the IEA's Net Zero roadmap. Emissions projections from the model are consistent with these scenarios but predict lower GDP growth. An alternative model version, assuming exponential energy efficiency improvement, produces GDP growth rates more in line with the benchmark projections. Our results imply that if internationally agreed net-zero objectives are to be fulfilled and economic growth is to follow SSP or IEA scenarios, then drastic changes in energy efficiency, not consistent with historical trends, are needed.

1 Introduction

Dramatically increasing amounts of energy have been produced and consumed worldwide since the pre-industrial era, which emit considerable amounts of greenhouse gases (GHGs), especially CO₂, into the atmosphere. The massive energy use has driven rapid economic expansion both globally and regionally. Going forward, it is desirable to maintain economic prosperity while addressing the concerning global warming issue due to increasing atmospheric GHG concentration levels. However, the E3-nexus, i.e., the interaction between energy consumption, environmental preservation, and economic development poses challenges ([Hamakawa, 2004](#); [Mitić et al., 2023](#)).

*Department of Economics and Business Economics, Aarhus University, Fuglesangs Allé 4, 8210 Aarhus V, Denmark.

As a response, the decoupling of economic growth from energy use and environmental impacts has come into focus in both academic research (e.g., [Stern, 2004b, 2004a](#); [Csereklyei & Stern, 2015](#); [Parrique et al., 2019](#); [Leitão et al., 2022](#)) and policy objectives such as the “Sustainable Development Goals” by the United Nations ([United Nations, 2015](#)).

In this paper, we consider CO₂ emissions as a proxy for environmental impacts. We specify a non-linear state space model of the energy, economy, and emissions nexus, abbreviated as E3S2 model, which is a state space system of consumptions of the five primary energy sources (coal, oil, gas, nuclear, and renewables), GDP, and CO₂ emissions.

The E3S2 model has several key features. First, it models time-varying emission factors. We represent CO₂ emissions as a weighted linear combination of fossil fuels. We allow the weights, emission conversion factors, to be time-varying. These factors are important because they affect the projection accuracy of CO₂ emissions from fossil fuel use. Although it is recognized that they can change over time (e.g., [Hong & Slatick, 1994](#); [Roten et al., 2022](#)), many factor estimates are dated, and hence alignment with current conditions is no longer guaranteed ([Omara et al., 2022](#); [Markovic et al., 2023](#)). We derive and estimate the time variations of the emission conversion factors from historical data, which sheds light on how technological improvements or changes in the composites of fossil fuels impact these factors.

Second, the E3S2 model captures non-stationarity. The predominant nature of non-stationarity in the observations of variables poses challenges for statistical inference. Conventional approaches of handling non-stationarity in the context of the economy-emissions-energy nexus mainly include various cointegration methods such as panel cointegration (e.g., [Hamit-Hagggar, 2012](#); [Lu, 2017](#); [Zoundi, 2017](#)), panel vector error correction models (e.g., [Pao & Tsai, 2010](#); [Apergis & Payne, 2009](#)), and autoregressive distributed lags (e.g., [Yue et al., 2021](#); [Adedoyin et al., 2021](#)). The state space methods employed in this paper allow for valid inference under non-stationarity ([Caines, 1988](#)). As a point of departure, we model the energy productivity factor, i.e., the reciprocal of energy intensity, and renewable energy consumption as a random walk with drift. Alternatively, a local linear trend form is employed if stochastic trends are found ([Durbin & Koopman, 2012](#)).

Third, the E3S2 model enables assessing parameter estimation uncertainty and incorporates both parameter and sampling uncertainty in the long-term projections and thus provides statistical confidence bands. A well-known class of models providing a comprehensive analysis of economy and environment is integrated assessment models (IAMs). IAMs adopt calibration to obtain parameter values and take averages of Monte Carlo runs of deterministic models with different parameter values drawn from a distribution to assess uncertainty ([Crost & Traeger, 2013](#); [Nordhaus, 2018](#)). However, as demonstrated by [Crost and Traeger \(2013\)](#), this approach can produce errors in both the magnitude and direction of the uncertainty. In contrast, state space techniques obtain estimates of the unknown parameters from data using maximum likelihood estimation and allow for standard statistical inference.

The remainder of the paper is structured as follows: Section 2 introduces the three modules of the E3S2 model. Section 3 describes the estimation of the E3S2 model using the extended

Kalman filter and presents the results from a Monte Carlo simulation study as a verification of the estimation procedure. Section 4 describes the data employed in this paper and introduces a data-driven model selection procedure. Section 5 presents the results of the estimation of the E3S2 model to both regional and global data. Section 6 presents long-term projections of CO₂ emissions, GDP, and the energy productivity factor conditional on the fuel mix pathways from the SSP 1.9 Wm⁻² scenario and the IEA Net Zero by 2050 roadmap. Section 7 concludes and discusses future research directions.

2 Specification of the E3S2 model

This section presents the general specification of the E3S2 model, which nests many choices of structures. The model can be estimated on data at global, regional, or country level. The E3S2 model consists of three modules: energy, emissions, and economy. The energy and emissions modules consist of linear equations, while the economy module contains a non-linear equation.

2.1 Energy

The energy module contains specifications for each type of energy carrier in the fuel mix. We treat coal, oil, gas, and nuclear energy as exogenously given and set them equal to their observations. In the following, capital letters with asterisk * denote unobserved state variables and the same letters without asterisk their corresponding data observations. We model the various energy carriers as follows:

$$\begin{aligned} C_t^* &= C_t, \quad O_t^* = O_t, \quad G_t^* = G_t, \quad N_t^* = N_t, \\ R_t^* &= d_{R,t-1} + R_{t-1}^* + \eta_{R,t-1}, \\ d_{R,t} &= d_{R,t-1} + \eta_{d_R,t-1}, \end{aligned} \tag{2.1}$$

where $(C_t, O_t, G_t, N_t, R_t)$ denote consumption quantities of the energy carriers coal, oil, gas, nuclear, and renewables, respectively. Renewable energy is specified as a random walk with time-varying drift. The drift process $d_{R,t}$ is a random walk itself, such that R_t is modeled as a local linear trend (Durbin & Koopman, 2012). The error processes $\eta_{R,t}$ and $\eta_{d_R,t}$ are the state disturbances of R_t^* and $d_{R,t}$, and they follow the normal distributions $\mathcal{N}(0, \sigma_{\eta_R}^2)$ and $\mathcal{N}(0, \sigma_{\eta_{d_R}}^2)$, respectively. If the variance $\sigma_{\eta_{d_R}}^2$ of the error process of the drift is zero, the drift is a constant, and R_t is a simple random walk with drift.

Treating the four fuel types (C_t, O_t, G_t, N_t) as exogenous (i.e., setting them equal to their observations) allows the use of the E3S2 model for projections using future energy pathways of different common scenarios such as SSPs or the IEA Net Zero roadmap. Modeling renewable energy instead of treating it as an exogenous variable not only allows for forecasting future renewable energy consumption conditional on trends inferred from historical data, but also facilitates conducting various scenario analyses regarding renewable energy, e.g., exploring the growth rate of renewable energy

2.2 Emissions

required to maintain a certain level of GDP growth when assuming all fossil fuels are phased out. See Section 6 for more details.

The energy module is completed by a measurement equation that specifies the observations of renewable energy as the state R^* plus a Gaussian error $\varepsilon_{R,t}$:

$$R_t = R_t^* + \varepsilon_{R,t}. \quad (2.2)$$

2.2 Emissions

We represent CO₂ emissions as a weighted average of consumptions of coal, oil, and gas (Marland & Rotty, 1984). The weights are the so-called emission conversion factors, which are the amounts of CO₂ released into the atmosphere from combustion of one unit of a given fossil fuel type. The emission module is specified as follows:

$$\begin{aligned} E_t^* &= \beta_{C,t}C_t^* + \beta_{O,t}O_t^* + \beta_{G,t}G_t^* + \eta_{E,t-1}, \\ \beta_{C,t} &= \beta_{C,t-1} + \eta_{\beta_C,t-1}, \\ \beta_{O,t} &= \beta_{O,t-1} + \eta_{\beta_O,t-1}, \\ \beta_{G,t} &= \beta_{G,t-1} + \eta_{\beta_G,t-1}, \end{aligned} \quad (2.3)$$

where $\eta_{E,t} \sim \mathcal{N}(0, \sigma_{\eta_E}^2)$. As specified in the first equation in system (2.1), we equate states with data for $C_t^* = C_t$, $O_t^* = O_t$, and $G_t^* = G_t$, and the data act as regressors for E_t^* . The coefficients $\beta_{.,t}$ denote the CO₂ emission conversion factors, which are time-varying and follow random walks, where $\eta_{\beta.,t} \sim \mathcal{N}(0, \sigma_{\eta_{\beta.}}^2)$. If the corresponding variances $\sigma_{\eta_{\beta.}}^2$ are set to or estimated as zero, the emission conversion factors are simply constants. Either constants or variances are estimated by maximum likelihood.

Allowing emission conversion factors $\beta_{.,t}$ to be time-varying is a key feature of the E3S2 model. Although a baseline value can be derived from physics, the factor can vary temporally or across different countries or regions. This can be caused by differences in the composites of the fuel product (Hong & Slatick, 1994; Roten et al., 2022) or by varying combustion efficiencies (Marland & Rotty, 1984). Ignoring substantial time-varying behavior can result in misspecification and residual autocorrelation in the equation for E_t^* . A time-varying specification can result in overfitting, however, if time variation is minimal (Roten et al., 2022).

The emissions module is completed by a measurement equation:

$$E_t = E_t^* + \varepsilon_{E,t}, \quad (2.4)$$

where E_t^* and E_t represent the state variable and observations of CO₂, respectively, and $\varepsilon_{E,t} \sim \mathcal{N}(0, \sigma_{\varepsilon_E}^2)$.

2.3 Economy

In the economy module, the macroeconomic output state variable, Y_t^* , is specified as the product of the aggregation of the energy mix and the energy productivity factor $\beta_{Y,t}$:

$$\begin{aligned} Y_t^* &= (C_t^* + O_t^* + G_t^* + N_t^* + R_t^*) \beta_{Y,t-1} + \eta_{Y,t-1}, \\ \beta_{Y,t} &= d_{\beta_Y,t-1} + \beta_{Y,t-1} + \eta_{\beta_Y,t-1}, \\ d_{\beta_Y,t} &= d_{\beta_Y,t-1} + \eta_{d_{\beta_Y},t-1}. \end{aligned} \tag{2.5}$$

The process $\beta_{Y,t}$ is a measure of energy efficiency or energy productivity, i.e., it quantifies the amount of GDP produced by a unit of the energy mix. Summation of energy consumption is based on the assumption that economic growth does not distinguish the source of energy, i.e., all energy types share the same per-unit contribution to GDP. (See, however, [Schurr and Netschert \(1960\)](#) for a discussion of substitution of fossil fuels of different qualities and the effect on energy efficiency.)

The residual processes $\eta_{Y,t}$, $\eta_{\beta_Y,t}$, and $\eta_{d_{\beta_Y},t}$ are assumed to be Gaussian following $\mathcal{N}(0, \sigma_{\eta_Y}^2)$, $\mathcal{N}(0, \sigma_{\eta_{\beta_Y}}^2)$, and $\mathcal{N}(0, \sigma_{\eta_{d_{\beta_Y}}}^2)$, respectively. Similar to R_t^* in Equation (2.1), $\beta_{Y,t}$ admits a flexible form of either a random walk ($\sigma_{\eta_{d_{\beta_Y}}}^2 = 0$) or a local linear trend ($\sigma_{\eta_{d_{\beta_Y}}}^2 > 0$). In the first equation in the system (2.5), $R_t^* \beta_{Y,t-1}$ is a product of two state variables, rendering the E3S2 model a non-linear state space model. The product of two random walk states allows capturing a large class of non-linear functions, see [Bennedsen, Hillebrand, and Koopman \(2023, Supplement S1\)](#).

The economy module is completed by a measurement equation that specifies GDP observations as their unobserved state counterpart plus Gaussian noise,

$$Y_t = Y_t^* + \varepsilon_{Y,t}. \tag{2.6}$$

In summary, the systems of equations (2.1), (2.3), and (2.5) comprise the non-linear state equations of the E3S2 model, and equations (2.2), (2.4), and (2.6) comprise the measurement equations.

3 Estimation and Monte Carlo simulation

As the E3S2 model is a non-linear Gaussian state space model, we apply the extended Kalman filter, which is an approximate filter. It linearizes the state equations and measurement equations using Taylor series and applies the Kalman filter to the linearized model. See [Durbin and Koopman \(2012\)](#) for a detailed description of the extended Kalman filter recursions. In Appendix B, we present the matrix form of the E3S2 model and the corresponding Jacobian matrix in the linearization of the non-linear state space model.

We estimate the parameters using maximum likelihood evaluated by the Kalman filter. We maximize the log-likelihood using the Nelder-Mead simplex search method in the R function “op-

tim” (Nelder & Mead, 1965). For non-stationary states, we adopt the “Big K” initialization technique to approximate the diffuse priors, where we set their initial variances to $K = 10^6$ (Durbin & Koopman, 2012). When an emission conversion factor is time-invariant, the corresponding state becomes a constant state, and we set the initial value of the mean to a constant and initial variance to zero. We conduct a Monte Carlo simulation study to assess the finite sample properties of the procedure. We consider the specification selected for OECD in Section 4 and a sample size of 49, which equals the length of the historical sample size. The data-generating parameters are set equal to the parameter estimates obtained from the data, see Table 5.1.

In this specification, we assume that the emission conversion factor of gas is time-varying, and the renewable energy state R^* admits a stochastic trend. The parameters for this model include time-invariant emission conversion factors β_C and β_O , the drift of β_{Y_t} , state disturbance variances $\sigma_{\eta_E}^2$, $\sigma_{\eta_Y}^2$, $\sigma_{\eta_{\beta_Y}}^2$, and $\sigma_{\eta_R}^2$, the variances of the error processes for the time-varying conversion factor of gas and stochastic trend of R^* , i.e., $\sigma_{\eta_{\beta_G}}^2$ and $\sigma_{\eta_{d_R}}^2$, and measurement error variances $\sigma_{\varepsilon_E}^2$, $\sigma_{\varepsilon_Y}^2$, and $\sigma_{\varepsilon_R}^2$.

Figure 3.1: Histogram of the differences of the parameter estimates from the data-generating parameter values in the Monte Carlo simulation. “dX” denotes the difference between the estimate of the parameter X and the corresponding data-generating value. The y-axis of each subfigure reports the relative frequencies. Solid yellow vertical lines and blue vertical lines represent the medians and means of dX, respectively.

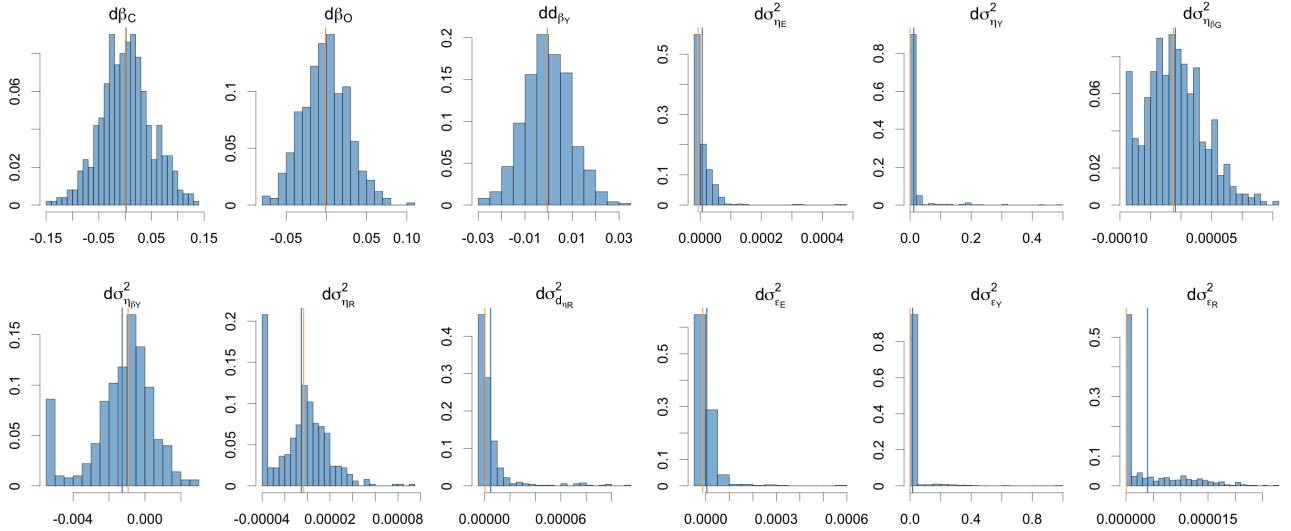


Figure 3.1 reports the distributions of parameter estimates in the Monte Carlo simulation across 500 runs. The differences $d\beta_C$, $d\beta_O$, and $dd\beta_Y$ of the parameter estimates from their data-generating values appear to be centered at zero and normally distributed. For the variances of state disturbances and measurement errors, the histograms cluster at zero, indicating that the model recovers the data-generating values despite their relatively small magnitudes. Note that there are clusterings at -0.004 and -0.00004 for $d\sigma_{\eta_{\beta_Y}}^2$ and $d\sigma_{\eta_R}^2$, as they are truncated to be non-negative in the algorithm and the data-generating values are 0.0053 and 0.000036, respectively. This is the

so-called "pile-up" issue (e.g., [Shephard, 1993](#)). In summary, the simulation exercise demonstrates that our estimation procedure has good finite-sample properties.

4 Data and model selection

4.1 Regions and data

We estimate the E3S2 model at both global and regional levels. For comparability with the regional analysis in SSPs, we adopt the region definition from the SSPs and consider the five regions OECD, REF, ASIA, MAF, and LAM, see Table 4.1 ([Riahi et al., 2017](#)).¹

Table 4.1: Five regions defined by SSPs.

Acronym	Description
OECD	OECD and European Union (EU) member states and candidates
REF	Eastern Europe and former Soviet Union
ASIA	most Asian countries (excl. the Middle East, Japan and former Soviet Union)
MAF	Middle East and Africa
LAM	Latin America and the Caribbean

We collect country-level and global-level data of CO₂ emissions from the Global Carbon Budget² ([Friedlingstein et al., 2022](#)) and of total energy supply³ from the International Energy Agency (IEA).⁴ Country-level GDP data are from the World Bank.⁵ We aggregate country-level data into regions. The five regions defined by SSP contain 190 countries in total, while due to the smaller data coverage of the energy dataset, we only include 146 countries in our analysis. See Appendix A for a list of countries that are excluded in this paper. The countries we do consider contribute approximately 96% of global emissions from fossil fuels.

The CO₂ emissions data are production-based emissions estimates from fossil fuels. They include emissions from fossil fuel combustion, oxidation, and cement production, and they exclude emissions from bunker fuels that are used for international aviation and maritime transport. Total energy supply data also exclude international marine and aviation bunkers. We use data series GDP (current local currency (LCU))(code: NY.GDP.MKTP.CN), Purchasing Power Parity (PPP) conversion factor (code: PA.NUS.PPP), and GDP deflator (code: NY.GDP.DEFL.ZS) to obtain GDP data measured in billions of 2005 USD (PPP adjusted). This enables the comparison of

¹A detailed list of countries in each region can be found at <https://tntcat.iiasa.ac.at/SspDb/dsd?Action=htmlpage&page=10#regiondefs>.

²<https://www.globalcarbonproject.org/carbonbudget/22/data.htm>, last accessed on October 2, 2023.

³Energy consumption data are not directly available. We use the total energy supply, which equals production + imports - exports - international marine bunkers - international aviation bunkers + stock changes.

⁴<https://www.iea.org/data-and-statistics/data-sets>, last accessed on September 29, 2023.

⁵<https://data.worldbank.org/indicator/NY.GDP.MKTP.CD>, last accessed on September 29, 2023.

4.1 Regions and data

GDP data across different years and different countries. We obtain GDP data at the global level by summing up the country-level series.

Figure 4.1: Data of the five main sources of primary energy (Panels (a) – (e)), CO₂ emissions (Panel (f)), and GDP (Panel (g)) during 1971 – 2019. The units of energy data and emissions data are million tonnes of oil equivalent and gigatonne (10⁹ tonne), respectively. The GDP data are in billion 2005 USD (PPP adjusted).

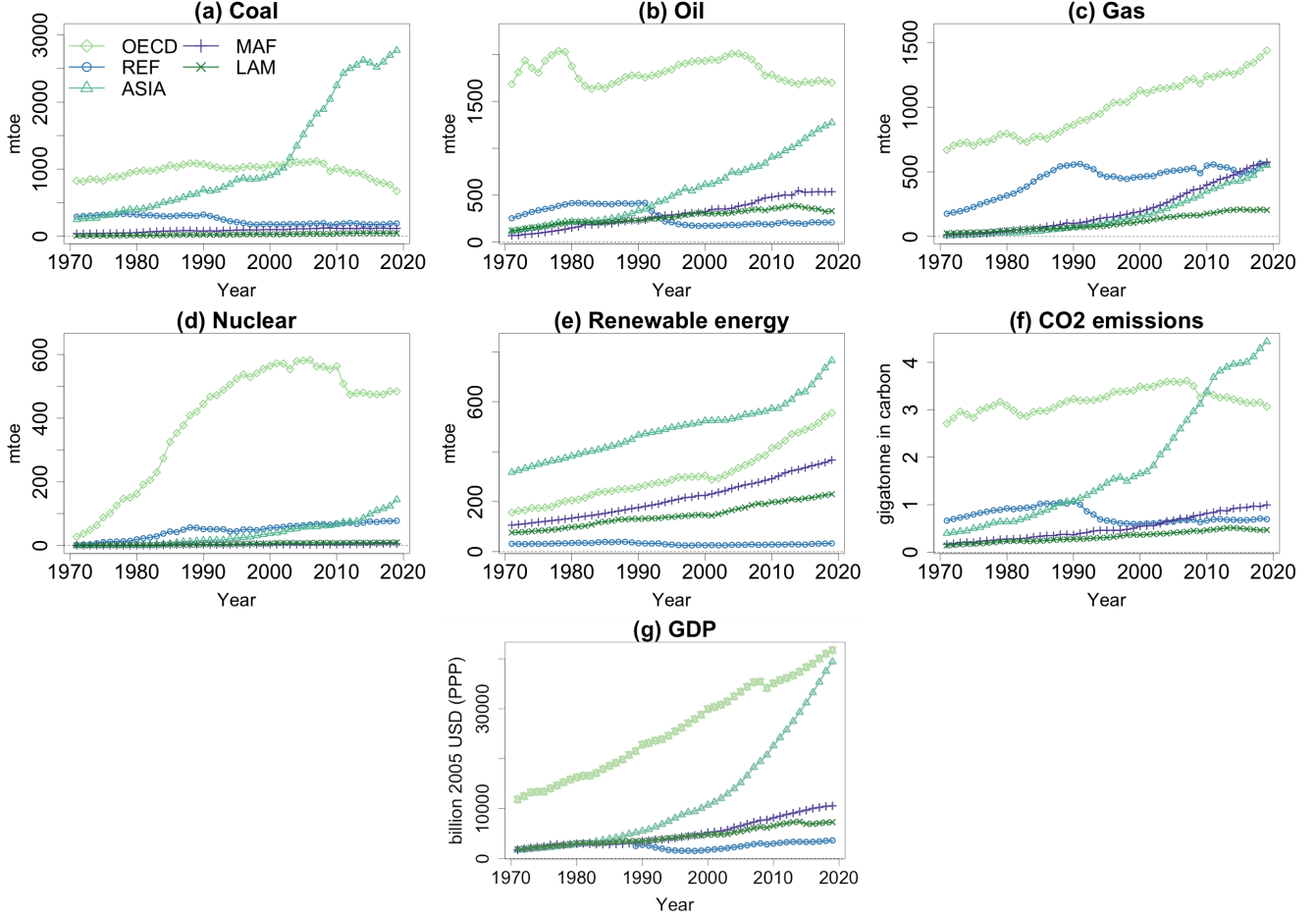


Figure 4.1 shows the data from 1971 to 2019, comprising 7 variables across 5 regions and the world. The data records for REF during 1971 – 1989 come from the region “Former Soviet Union” in the IEA database. This region includes 15 post-Soviet countries, while REF includes only 12 post-Soviet countries.⁶ In Panels (a) – (e) in Figure 4.1, the five main sources of primary energy have been transformed to the same unit of million tonnes of oil equivalent (mtoe).

In terms of regional magnitudes of energy use, as shown in Panels (a), (b), and (d), the OECD region has been the largest consumer of oil, gas, and nuclear energy, and it used to be the leading coal consumer until it was overtaken by ASIA in 2003, which continuously experiences high growth rates in coal usage afterward. The total supplies of coal and oil in the OECD region have shown a decreasing trend since 2008 and 2006, respectively. This is in line with the observation that CO₂ emissions in Panel (f) start to decline in the same period. Meanwhile, as shown in Panel (g),

⁶Estonia, Latvia, and Lithuania are European Union (EU) member countries and are included in region OECD.

Table 4.2: Share of each energy type in percentages for the five regions and the world in 2019. The values of each row sum up to 100.

Region	Coal	Oil	Gas	Nuclear	Renewable
OECD	13.92	35.03	29.64	9.97	11.44
REF	17.87	19.65	52.14	7.27	3.08
ASIA	50.36	23.13	10.00	2.61	13.90
MAF	7.32	33.53	35.94	0.31	22.90
LAM	5.36	40.45	24.97	1.14	28.07
WORLD	26.67	31.42	23.17	5.02	13.72

GDP in the OECD region continuously grows with the exception of two years due to the financial crisis. This is a sign of decoupling of economic growth and emissions, i.e., CO₂ emissions decrease, while economic growth continues.⁷ Renewable energy use has increased for all regions, with ASIA and OECD experiencing accelerating growth after 2000, MAF and LAM visually linear growth, and REF remaining relatively constant. At the global level, all of the seven variables are trending upward over the sample period, with renewable energy and GDP rising at increasing rates over the past two decades.

Table 4.2 presents the contributions in percentage from each of the primary energy sources for the five regions and the world in 2019. Fossil fuels are still the major source of energy for the world (taking up more than 80%) and all regions up to 2019. Coal is the largest contributor for ASIA, oil for OECD and LAM, and gas for REF and MAF. Notably, more than a quarter of the primary energy in LAM comes from renewables. Renewable energy also takes up a high share in MAF, as many African countries are abundant in renewables such as sunlight (Cozzi et al., 2022).

4.2 Model selection

As shown in Figure 4.1, the primary energy supplies, CO₂ emissions, and GDP exhibit different characteristics across regions. Therefore, it is not feasible to incorporate all these features in a single statistical model simultaneously. In this section, we introduce a data-driven model selection procedure. It starts from a base model without time-varying parameter processes and hones in on a specification appropriate for the regional data. We estimate the base model and test the residuals for serial correlation to decide which parameters to specify as time-varying.

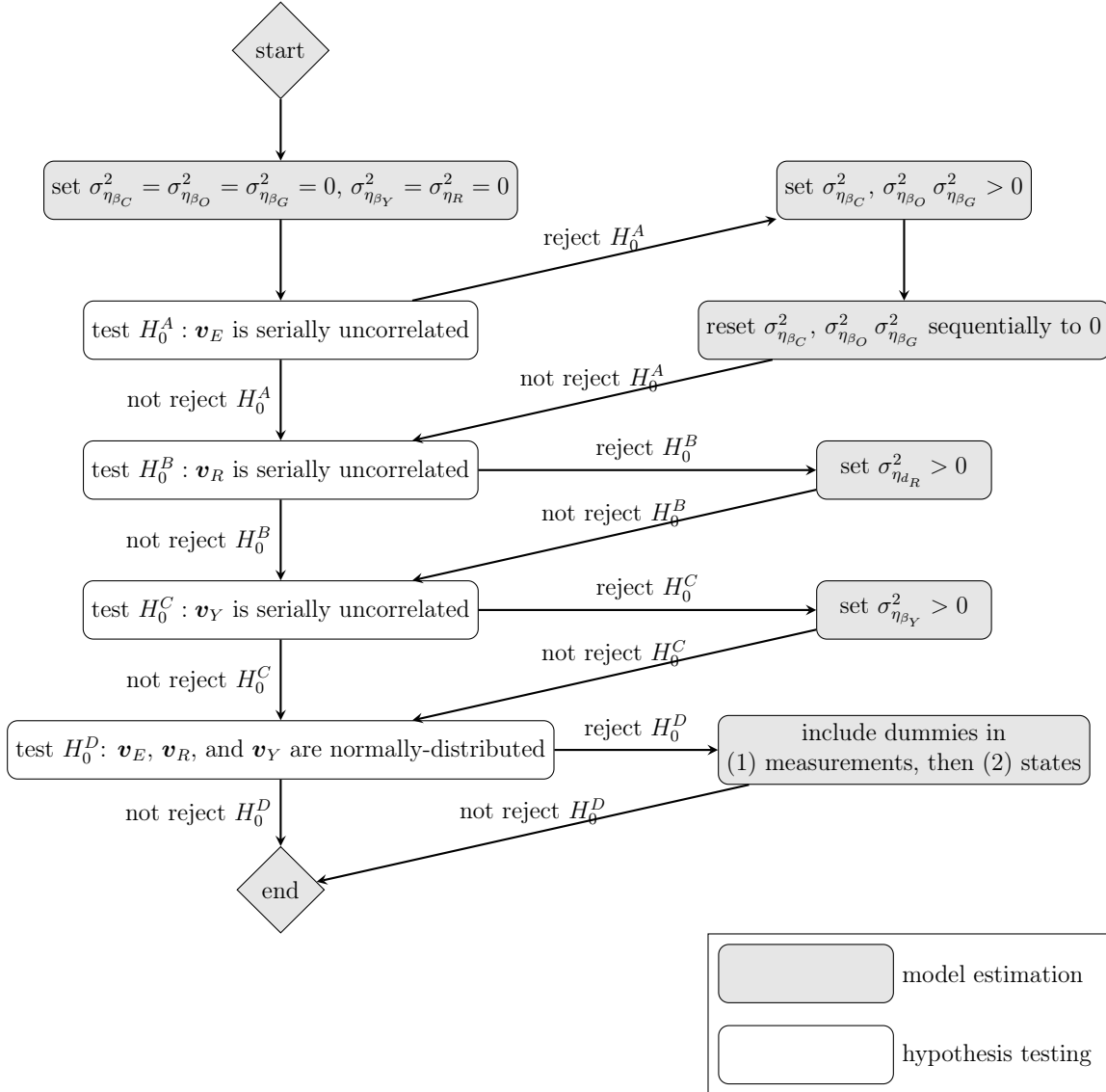
Figure 4.2 presents a diagram of the model selection procedure. The point of departure is the base specification estimated on the data, and four hypothesis tests A, B, C, and D are conducted sequentially on the residuals, which are the standardized one-step ahead prediction errors series \mathbf{v}_X , where $X \in \{E, Y, R\}$. The first three hypothesis tests A, B, and C are Ljung-Box tests for

⁷This finding, however, does not hold true for consumption-based emissions, see Bennedsen, Hillebrand, and Jensen (2023).

4.2 Model selection

autocorrelation (Box & Pierce, 1970; Ljung & Box, 1978). We consider lag orders 1 and 5 and significance levels 1% and 5%. The null hypothesis H_0 is the absence of serial correlation. If the null of test A, H_0^A , is rejected, constant emission conversion factors cannot capture changes in the relationship between emissions and fossil fuel consumption. Then, all conversion factors are set to be time-varying, and the model is re-estimated. The smoothed conversion factors that remain almost constants are reset to constants. The procedure is repeated until we find a specification where H_0^A cannot be rejected.

Figure 4.2: Flow chart of the data-driven model selection procedure



In tests B and C, we test whether autocorrelation remains in the residuals of renewables and GDP, respectively. Upon rejection of the null we incorporate a stochastic trend for R^* in Equation (2.1) or/and β_Y in Equation (2.5). We test v_R first because R^* is an element in the equation for GDP. Modeling R^* using a local linear trend model can help remove autocorrelation in the residuals of GDP, if R^* is the only source of a stochastic trend in GDP.

Test D employs the Jarque-Bera (Jarque & Bera, 1980) test for non-normality of the three residual processes v_E , v_Y , and v_R . In case of rejection, we introduce dummy variables for large spikes first in the corresponding measurement equations, then in the state equations, until the test fails to reject. We ignore the issue of multiple testing since the nominal size of the tests in this model building cycle is not material.

We apply the model selection procedure to the five regions and the world and obtain a specification for each. Table 4.3 summarizes the specifications. Note that four types of specifications

Table 4.3: Summary of specifications nested in the general form of E3S2 model. “o” indicates a particular structure is needed. “LL” denotes the local linear trend model ($\sigma_{\eta_{\beta_Y}}^2, \sigma_{\eta_R}^2 > 0$).

Region	time-varying β_C	time-varying β_O	time-varying β_G	LL in β_Y	LL in R^*	No. of dummies
World	o			o	o	3
OECD			o		o	1
REF	o			o		0
ASIA	o			o	o	2
MAF	o			o	o	6
LAM	o					0

are selected: (i) β_C is time-varying, (ii) β_C is time-varying, β_Y is local linear trend, (iii) β_G is time-varying, R^* is local linear trend, and dummy variables are added, (iv) β_C is time-varying, both β_Y and R^* are local linear trends, and dummy variables are added.

5 Estimation on global and regional data

Employing the specifications selected in Section 4.2, we fit the models to the data series for each region and estimate the parameters using maximum likelihood via the output from the extended Kalman filter. Table 5.1 presents the results, where we estimate the regionally averaged and globally averaged conversion factors empirically.⁸ Emission conversion factors represent the amount of CO₂ emissions per unit of combusted energy carrier; smaller values indicate that the energy carrier is less polluting.

Table 5.1 shows that the majority of time-invariant emission conversion factor estimates are in line with numbers reported in the literature and presented in Panel E. Emission conversion factor estimates vary across regions, consistent with the statements in Hong and Slatick (1994) and Roten et al. (2022). An exception is ASIA with a higher $\hat{\beta}_O$ and lower $\hat{\beta}_G$, but these two estimates also have larger standard errors. Considering the uncertainty and confidence intervals, they are in good agreement with the benchmarks.

⁸We refrain from reporting the estimated variances. They are available upon request.

Table 5.1: Point estimates and standard errors (in parentheses) of CO₂ emission conversion factors β_C , β_O , and β_G , drifts d_{β_Y} and d_R , and coefficients of dummies D . The superscript of D indicates whether the dummy is included in the state equation (S) or the measurement equation (M), and the subscript refers to the variable name and time index of the dummy. Emission conversion factors are expressed in units of tonne CO₂ equivalent per tonne of oil equivalent (tonne CO₂e/ toe). Estimates of the time-varying emission conversion factors (labeled “TV”) are reported in the figure below the table. Panel E reports the emission conversion factor estimates from [Marland and Rotty \(1984\)](#) and IPCC emission factor database ([Mangino et al., 2002](#)) for comparison.

A. β_C is time-varying									
	$\hat{\beta}_C$	$\hat{\beta}_O$	$\hat{\beta}_G$	\hat{d}_{β_Y}	\hat{d}_R				
LAM	TV	3.3775 (0.2291)	2.3005 (0.3002)	0.0196 (0.0199)	0.0032 (0.0004)				
B. β_C is time-varying and β_Y has a local linear trend form									
	$\hat{\beta}_C$	$\hat{\beta}_O$	$\hat{\beta}_G$	\hat{d}_R					
REF	TV	3.7799 (1.6623)	1.9663 (0.3399)	0.00004 (0.0002)					
C. β_G is time-varying, R^* has a local linear trend form, and dummies needed									
	$\hat{\beta}_C$	$\hat{\beta}_O$	$\hat{\beta}_G$	\hat{d}_{β_Y}	$\hat{D}_{E,1990}^S$				
OECD	3.9852 (0.5086)	2.6785 (0.2098)	TV	0.1075 (0.0106)	0.036 (0.009)				
D. β_G is time-varying, β_Y and R^* have a local linear trend form, and dummies needed									
	$\hat{\beta}_C$	$\hat{\beta}_O$	$\hat{\beta}_G$	$\hat{D}_{E,2004}^S$	$\hat{D}_{E,1990}^M$				
ASIA	TV	4.2428 (1.9129)	1.3744 (2.473)	-0.0778 (0.0227)	-0.0809 (0.0119)				
	$\hat{\beta}_C$	$\hat{\beta}_O$	$\hat{\beta}_G$	$\hat{D}_{Y,1982}^S$	$\hat{D}_{R,2000}^M$	$\hat{D}_{R,2004}^M$	$\hat{D}_{R,2011}^M$	$\hat{D}_{R,2012}^M$	$\hat{D}_{R,2013}^M$
MAF	TV	1.918 (1.2612)	2.992 (0.7784)	-0.1103 (0.0834)	-0.0026 (0.0007)	0.0014 (0.0007)	0.0017 (0.0009)	0.0053 (0.0010)	0.0040 (0.0009)
	$\hat{\beta}_C$	$\hat{\beta}_O$	$\hat{\beta}_G$	$\hat{D}_{E,1991}^S$	$\hat{D}_{Y,1990}^S$	$\hat{D}_{Y,1989}^M$			
WORLD	TV	2.8984 (0.4132)	2.8848 (0.4328)	0.149 (0.020)	1.0447 (0.2531)	1.1089 (0.2612)			
E. Emission conversion factor estimates from other literature									
				$\hat{\beta}_C$	$\hat{\beta}_O$	$\hat{\beta}_G$			
Marland and Rotty (1984)				2.6841	2.8590	2.0560			
Mangino et al. (2002) ^a				4.1112	3.0681	2.3470			

^a IPCC emission factor database (EFDB).

Smoothed states of the time-varying emission conversion factors. Confidence bands are pointwise at the 90% level.

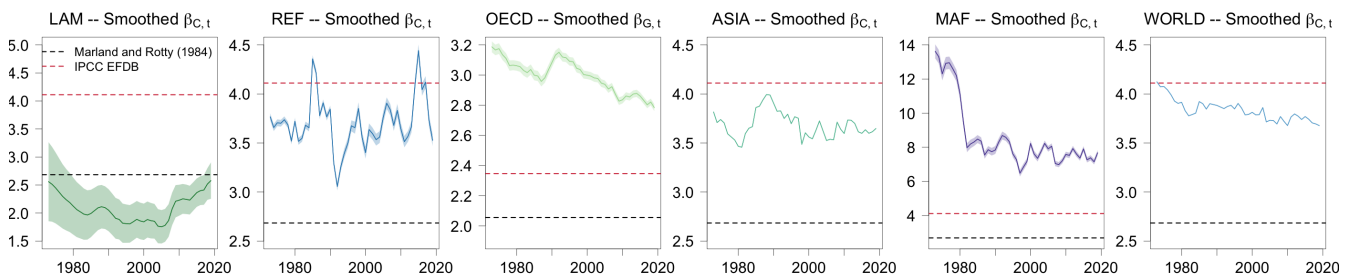


Table 5.3: Diagnostic statistics of the standardized one-step ahead prediction errors of emissions, GDP, and renewables. It reports the first four moments (mean, standard deviation (Std), skewness (Skew), and excess kurtosis (Kurt) as well the test statistics of the Jarque-Bera test for non-normality (Jarque & Bera, 1980) (JB) and of the Ljung-Box test for autocorrelation (Box & Pierce, 1970; Ljung & Box, 1978) (Q(1) corresponds to a lag order of 1 and Q(5) corresponds to a lag order of 5.) We consider significance levels of 1% (**) and 5% (*). The null hypothesis of the Jarque-Bera is skewness equal 0 and kurtosis equal 3. The null hypothesis of the Ljung Box test is that the residuals are serially uncorrelated when a fixed number of lags are included.

A. β_C is time-varying								
		Mean	Std	Skew	Kurt	JB	Q(1)	Q(5)
LAM	Emissions	-0.113	0.993	0.435	-0.294	1.673	2.331	3.889
	GDP	0.000	1.000	-0.229	0.225	0.712	0.780	3.255
	Renewables	0.001	1.011	0.158	-0.633	0.779	1.779	7.673
B. β_C is time-varying, and β_Y has a local linear trend form								
		Mean	Std	Skew	Kurt	JB	Q(1)	Q(5)
REF	Emissions	-0.027	1.000	0.220	0.905	2.714	0.177	5.108
	GDP	-0.035	0.977	-0.648	-0.202	2.391	0.723	5.653
	Renewables	0.001	1.011	-0.461	0.502	2.659	0.702	3.993
C. β_G is time-varying, R^* has a local linear trend form, and dummies needed								
		Mean	Std	Skew	Kurt	JB	Q(1)	Q(5)
OECD	Emissions	-0.266	0.963	0.200	-0.891	1.624	0.278	3.814
	GDP	0.016	0.957	0.283	-0.075	0.686	2.498	4.326
	Renewables	0.123	0.992	-0.095	0.561	1.097	0.064	1.109
D. β_C is time-varying; β_Y and R^* have local linear trend form, and dummies needed								
		Mean	Std	Skew	Kurt	JB	Q(1)	Q(5)
ASIA	Emissions	-0.043	0.999	-0.040	0.973	2.629	0.317	4.164
	GDP	0.027	0.983	0.256	0.553	1.554	1.127	6.273
	Renewables	0.169	0.983	0.106	0.609	1.264	0.007	13.553*
MAF	Emissions	-0.183	0.983	-0.733	0.303	4.976	0.997	2.634
	GDP	-0.016	0.988	-0.088	0.902	2.355	0.260	1.481
	Renewables	0.169	0.987	-0.334	0.951	3.464	0.053	18.945**
WORLD	Emissions	-0.203	0.979	0.212	0.949	2.888	1.550	9.694
	GDP	0.053	0.974	0.415	0.095	1.569	0.254	9.433
	Renewables	0.181	0.984	0.210	-0.291	0.437	0.019	2.148

Five out of six time-varying emission factors are moving within the ranges comparable to the benchmarks of either Marland and Rotty (1984) or the IPCC emission factor database (EFDB) (Mangino et al., 2002). MAF has a high estimated $\beta_{C,t}$ starting from over 12 tonnes CO₂e/ toe but rapidly falling to eight. LAM, MAF, and WORLD exhibit downward trends in $\beta_{C,t}$, indicating “cleaner” coal usage in terms of CO₂ emissions over the years. The decreasing smoothed $\beta_{G,t}$ suggests gas becomes less polluting over time in the OECD region.

Table 5.3 reports diagnostics on the residuals to evaluate the performance of the model fits. Except for ASIA and MAF where autocorrelation cannot be rejected at a lag order of 5, all the other residual processes appear to be normally distributed and serially uncorrelated. This indicates that the specifications provide a good fit to the data, and no missing dynamics need to be accounted for. The smoothed states and residuals are shown in Appendix C.

Figure 5.1: CO₂ emissions (y-axis, gigatonne in carbon) against GDP (x-axis, billion 2005 USD (PPP)). The solid lines represent smoothed states, while circles represent historical data.

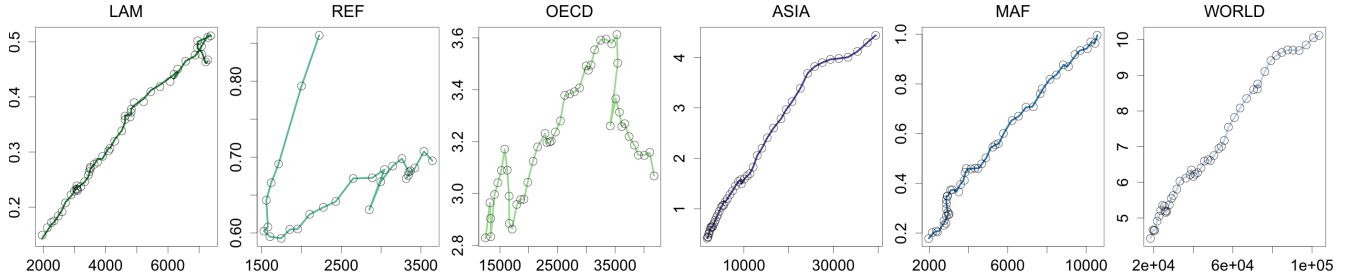


Figure 5.1 shows the smoothed states and historical data of CO₂ emissions on the y-axis and of GDP on the x-axis. For the OECD region, the graph shows an inverse U-shape. This is the environmental Kuznets curve (EKC), reflecting a relationship between economic growth and environmental impact (Grossman & Krueger, 1991; Castle & Hendry, 2020), here estimated from the output of the Kalman smoothing recursions. The hypothesis is that in the early stages of economic growth, environmental externalities increase, in this case increases in CO₂ emissions. Once a turning point is reached, economic expansion improves environmental quality. Note that CO₂ emissions data employed in this paper are production-based. None of the other regions display an EKC shape. The picture for the OECD changes when using consumption-based data, as discussed in Bennedsen, Hillebrand, and Jensen (2023).

6 Scenario analysis

In this section, we conduct scenario analysis with the E3S2 model conditional on energy pathways from the SSPs and the IEA Net Zero Roadmap.

6.1 Long-term projections

We perform statistical projections of CO₂ emissions and GDP with the E3S2 model, using the estimated parameters from the empirical exercise in Section 5 for each region. Fossil and nuclear energy sources are exogenous in the E3S2 model. In the projection, they are given by the fuel mix series from SSP 1.9 Wm⁻² (shown in Figure 6.1).

In contrast to IAMs, we consider parameter uncertainty and construct confidence bands accordingly. We start with the vector of five parameters $\theta = (\beta_C, \beta_O, \beta_G, d_{\beta_Y}, d_R)'$. We randomly draw

a vector of parameters from the distribution $\mathcal{N}(\hat{\boldsymbol{\theta}}, \hat{\boldsymbol{\Omega}})$, where $\hat{\boldsymbol{\theta}}$ denotes the estimated mean of $\boldsymbol{\theta}$ and $\hat{\boldsymbol{\Omega}}$ denotes the estimated variance-covariance matrix of $\boldsymbol{\theta}$, respectively. We insert the drawn parameter vector into the model and keep other parameters such as variances of measurement errors constant at their point estimates. For time-varying emission conversion factors, we set the mean and the variance to their smoothed values in 2019. For β_Y and R_t , we set the mean and variance equal to the median from the period 2015-2019. As the SSP database does not contain confidence bands of the energy pathways, we do not consider uncertainty of the energy trajectories. We extract the filtered states of E^* and Y^* conditional on the SSP 1.9 Wm^{-2} energy trajectories as projected emissions and GDP over the period 2020 – 2100 at a 10-year frequency. We iterate this process and generate 10,000 trajectories. From these, we obtain the 5th percentile, the median, and the 95th percentile, from which we draw the 90% confidence bands. These confidence bands capture parameter estimation uncertainty from the draw of the parameter vectors and sampling uncertainty from the 10,000 Monte Carlo simulations. In Sections 6.2 and 6.3, we present the scenario analysis at both the regional and global levels.

6.2 Regional scenario analysis conditional on SSP 1.9 Wm^{-2}

6.2.1 SSP 1.9 Wm^{-2}

The SSP scenarios provide a framework of five narratives with distinct socio-economic assumptions for the future until 2100 to complement the GHG concentration trajectories from the Representative Concentration Pathways. The five storylines are labeled: SSP1 – sustainability, SSP2 – middle of the road, SSP3 – regional rivalry, SSP4 – inequality, and SSP5 – fossil-fueled development.

Six IAMs participate in quantifying the SSP narratives: the Asia-pacific Integrated Model (AIM) (Fujimori et al., 2017); the Global Change Assessment Model (GCAM4) (Calvin et al., 2017); the Integrated Model to Assess the Global Environment (IMAGE) (Van Vuuren et al., 2017); the Model for Energy Supply Strategy Alternatives and their General Environmental Impact combined with the Global Biosphere Management Model (MESSAGE-GLOBIOM) (Fricko et al., 2017); the Regionalized Model of Investments and Development combined with the Model of Agricultural Production and its Impact on the Environment (REMIND-MAGPIE) (Kriegler et al., 2017); and the World Induced Technical Change Hybrid model combined with GLOBIOM (WITCH-GLOBIOM) (Emmerling et al., 2016). Each SSP storyline is implemented in multiple IAMs, and one of the IAMs is selected as a representative “marker” of the narrative. Within each of the main SSP storylines 1–5, different scenarios for radiative forcing levels by 2100 are considered, some aligning with the goals of the Paris Agreement, others not.

In this paper, we focus on the 1.9 Wm^{-2} scenario, which restricts radiative forcing level to 1.9 Wm^{-2} by the end of the twenty-first century. Under this scenario, the goal set by the Paris Agreement to limit the global mean temperature rise relative to the pre-industrial level below 1.5 °C is achievable (Rogelj et al., 2018). Across all 1.9 Wm^{-2} scenarios, the probability of limiting peak warming below 1.5 °C ranges from 20% to 48%, with the probability inversely related to

yearly GHG emissions in 2030 (Rogelj et al., 2018).

Following Rogelj et al. (2018), we use the name SSPx-1.9, where $x \in \{1, 2, 3, 4, 5\}$ refers to the specific SSP storyline. Note that due to high regional heterogeneity, all models under SSP3 fail to generate a solution that achieves limiting the end-of-century forcing to $1.9 Wm^{-2}$. The goal is also challenging for SSP4 and SSP5, although it is reached by the marker model in SSP5 (Rogelj et al., 2018). For this reason, we restrict our focus to SSP1-1.9, SSP2-1.9, and SSP5-1.9.

Table 6.1: Key energy characteristics for the marker in SSP 1.9 Wm^{-2} scenario (Rogelj et al., 2018). Non-biomass renewables include solar, wind, hydro and geothermal energy.

Scenario	SSP1-1.9	SSP2-1.9	SSP5-1.9
Narrative	Sustainability	Middle of the road	Fossil-fueled development
Marker Scenario	IMAGE	MESSAGE-GLOBIOM	REMIND-MAGPIE
Fossil fuels	phase-out	phase-out	phase-out
Final energy reduction over 2020 – 2100 relative to the baseline	37%	30%	34%
Global annual final energy intensity rate of change over 2020 – 2050	-0.9%	-1.2%	-1.4%
Share of non-biomass renewables in 2050	23%	32%	24%
Share of non-biomass renewables in 2100	30%	55%	54%

Table 6.1 presents an overview of some key features of the energy sector for SSP1-1.9, SSP2-1.9, and SSP5-1.9, where the marker scenario achieves the goal of $1.9 Wm^{-2}$. Despite SSP5-1.9 having a fossil-fueled storyline, it assumes a phase-out of all fossil fuels and the largest annual reduction in energy intensity. SSP1-1.9 features the highest final energy reduction, aligning with its core narrative of adopting a sustainable path. All scenarios exhibit an increase in the share of non-biomass energy (e.g., Creutzig et al., 2015).

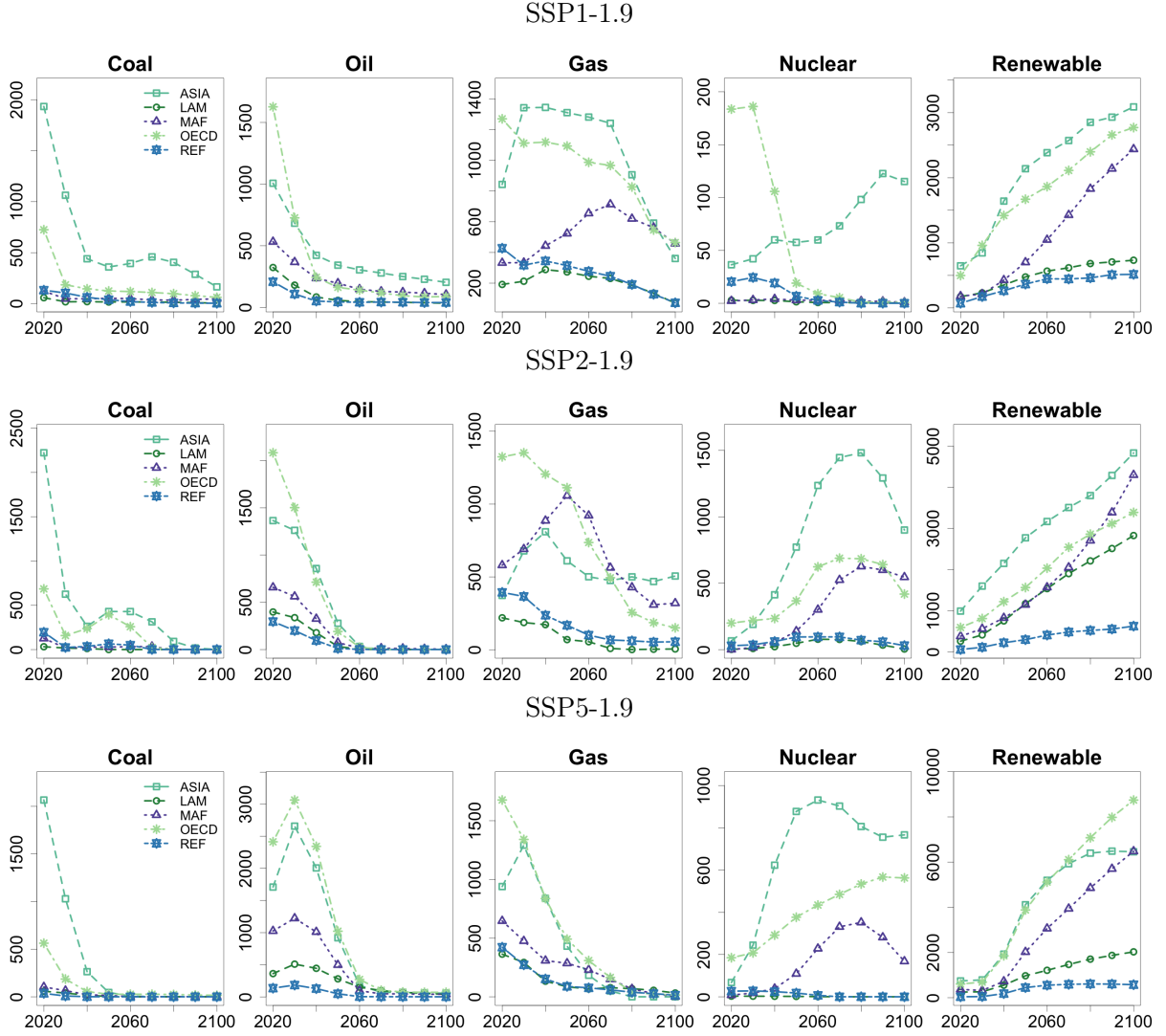
We collect SSP 1.9 projections of the energy mix at a regional level from the SSP Database (Rogelj et al., 2018). The regional realizations of each energy source are generally in line with the key features in Table 6.1. All regions shift away from fossil fuels and exhibit rapid scale-up in renewable energy use. However, SSP1-1.9 and SSP2-1.9 do not completely phase out fossil fuels for some regions. For instance, ASIA still uses a small amount of coal and oil by the end of the century, mostly with abatement (i.e., with carbon capture and storage, CCS). SSP1-1.9 deviates considerably from other two scenarios in nuclear energy use. Four out of the five regions in SSP1-1.9 phase out nuclear energy in the period 2050 – 2070, including OECD, whereas in SSP2-1.9 and SSP5-1.9, the regions OECD, ASIA, and MAF initially increase nuclear use and reduce only later towards the end of the century.

6.2.2 Projections with linear growth in energy productivity

We follow the approach described in Section 6.1 and generate projections from the E3S2 model. For the time-varying emission conversion factors, we use the smoothed values from 2019 and assume them as constant conversion factors in the projection. If β_Y is found to have a stochastic trend

6.2 Regional scenario analysis conditional on SSP 1.9 Wm^{-2}

Figure 6.1: SSP 1.9 Wm^{-2} projections of primary energy use (unit: million tonnes of oil equivalent (mtoe)) at 10-year frequency over the period 2020 – 2100 (Rogelj et al., 2018).

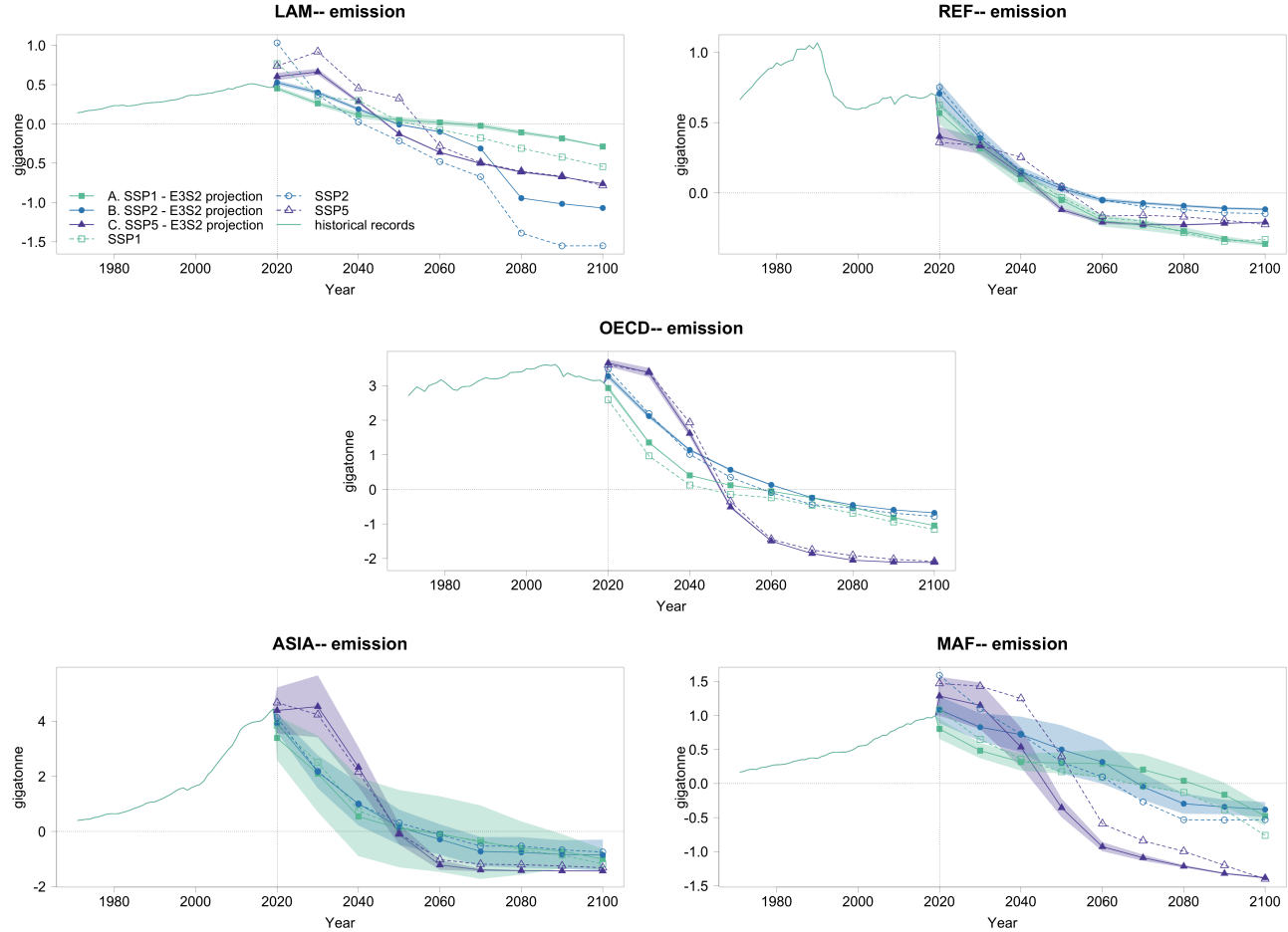


$d_{\beta_Y, t}$, we calculate the median of the smoothed $d_{\beta_Y, t}$ over the five-year period 2015 – 2019 and assume it as the linear trend slope for β_Y in the future. The same approach is used if R^* is found to have a stochastic trend.

Figure 6.2 presents model-projected CO_2 emissions compared to the emissions trajectories from SSP1-1.9, SSP2-1.9, and SSP5-1.9 marker scenarios. As the SSP trajectories are adjusted by CCS, and this is not featured in our model, we collect the SSP CCS pathways and subtract them from our model output to obtain projections comparable to the SSP trajectories. As shown in Figure 6.2, the CO_2 emissions projections generated from the E3S2 model have good agreement with the SSP 1.9 trajectories. LAM and MAF exhibit some discrepancies, primarily because our datasets cover fewer countries than the SSP scenarios for these regions. ASIA shows a wider 90% confidence band compared to other regions, reflecting larger uncertainty in the emission conversion factors

(Table 5.1).

Figure 6.2: Comparison of CO₂ emissions projected by the E3S2 model plus carbon capture and storage (CCS) from SSP scenarios and CO₂ projections under SSP 1.9 Wm^{-2} scenarios. Confidence bands are pointwise at the 90% level.

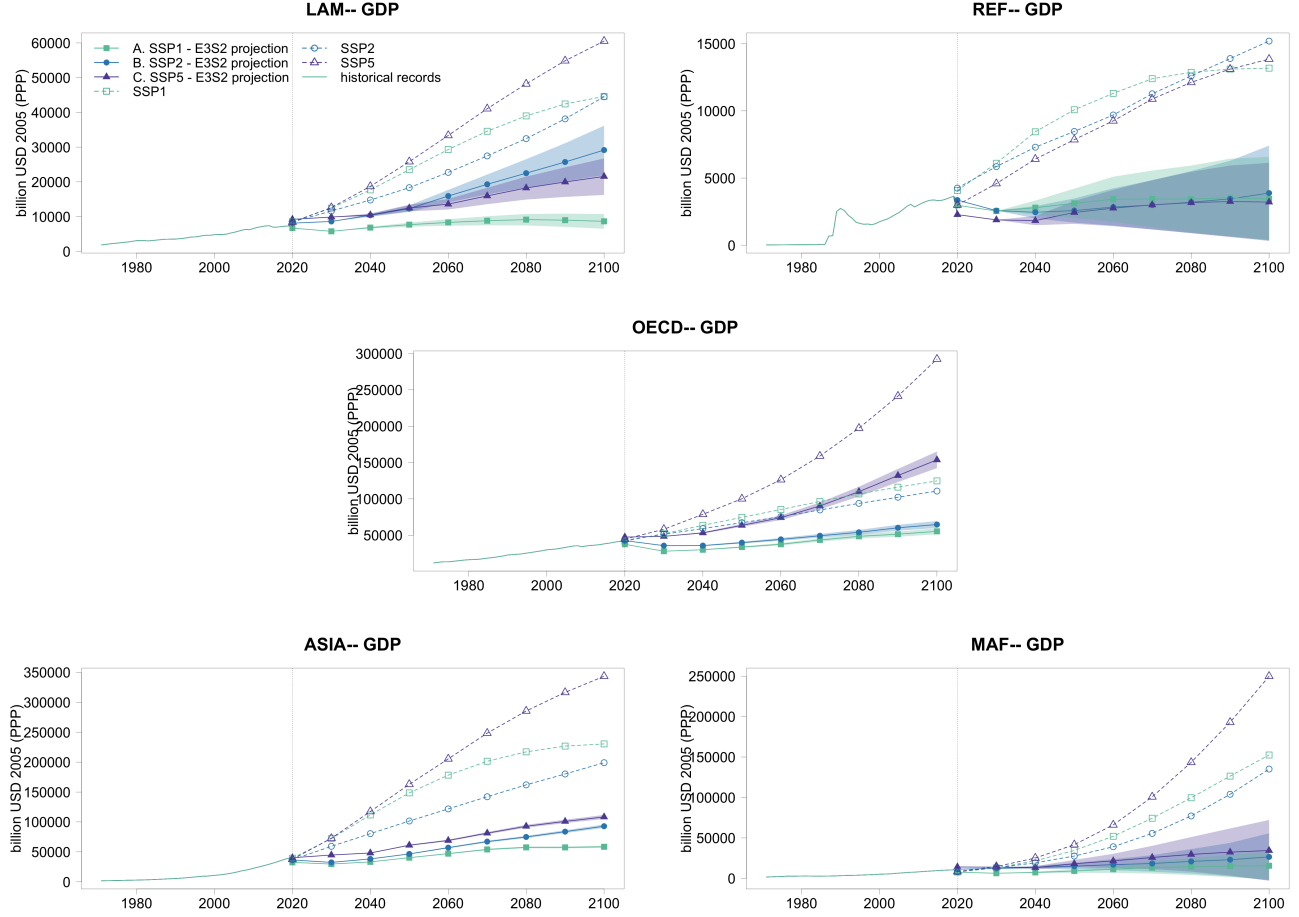


While our emissions projections largely agree with those from the SSP scenarios, our GDP projections appear considerably lower than the SSP projections, as illustrated in Figure 6.3. The significant discrepancies arise from differences in the fundamental assumptions and methodologies between our approach and the SSP studies.

Three models perform the economic projection for the SSPs. These models are developed by research teams from the International Institute for Applied Systems Analysis (IIASA) (Cuarema, 2017), the Organization for Economic Co-operation and Development (OECD) (Dellink et al., 2017), and the Potsdam Institute for Climate Impact Research (PIK) (Leimbach et al., 2017), respectively. All three models share the harmonized assumptions regarding the main drivers of economic growth but they differ in methodology.

For example, the ENV-Growth model adopts the “conditional convergence growth” methodology (Dellink et al., 2017), wherein energy functions both as a production input and as an income generator, particularly for countries rich in oil and gas. The model assumes that the energy effi-

Figure 6.3: Comparison of GDP projected by the E3S2 model and GDP under SSP 1.9 Wm^{-2} scenarios. Confidence bands are pointwise at the 90% level.



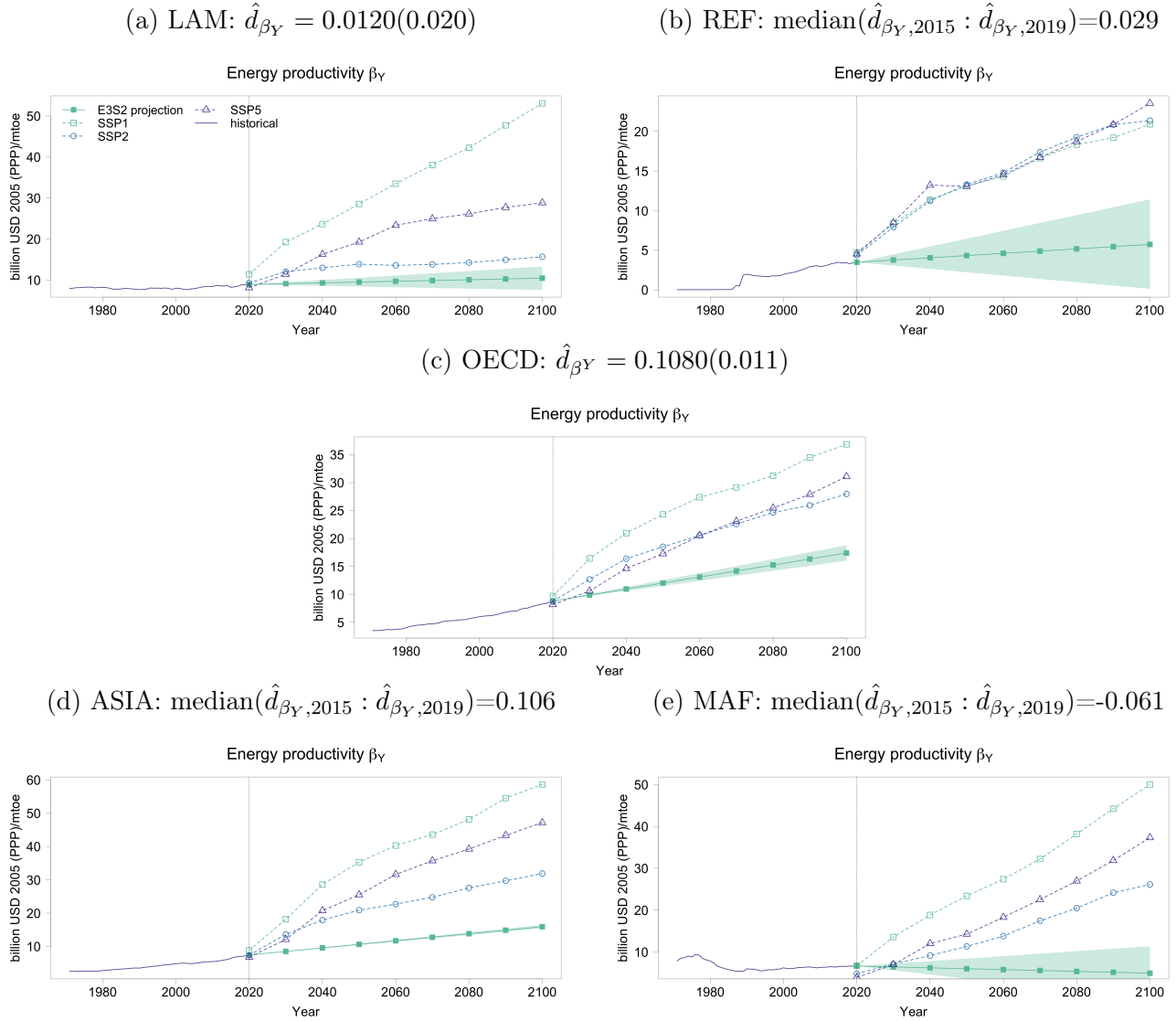
ciency of each country (equivalent to the energy productivity in our paper) drives energy demand and converges to that of the leading economies in the projection. There are six factors contributing to long-term economic growth: physical capital, employment, human capital, energy demand, extraction and processing of the fossil fuel resources oil and gas, and total factor productivity. The model is then calibrated using historical data. The ENV-Growth model incorporates numerous determinants of the economy, along with various assumptions on endogenous convergence mechanisms and exogenous factors across regions. Consequently, the projections are subject to a high level of uncertainty (Dellink et al., 2017).

In our model, time-varying energy productivity captures changes in technology. We model energy productivity (β_Y in Equation (2.6)) either as a deterministic trend ($\sigma_{\beta_Y}^2 = 0$) or a stochastic trend ($\sigma_{\beta_Y}^2 > 0$). In the projections, β_Y is the only endogenous factor determining economic growth when all energy source series are given from SSP scenarios. The dynamics of β_Y are inferred statistically from historical data as shown in Table 5.3.

Figure 6.4 shows that the energy productivity implied by the SSP projections, calculated by

6.2 Regional scenario analysis conditional on SSP 1.9 Wm^{-2}

Figure 6.4: Comparison of β_Y projected by the E3S2 model with β_Y implied by SSP 1.9 projections. The title of each panel reports the region and the estimated growth rate of β_Y . For REF, ASIA, and MAF, where β_Y follows a local linear trend model, we use $\text{median}(\hat{d}_{\beta_Y,2015} : \hat{d}_{\beta_Y,2019})$, which represents the median of the smoothed $d_{\beta_Y,t}$ over 2015 – 2019, as the linear trend for β_Y in the projection. Confidence bands are pointwise at the 90% level.



dividing SSP-projected GDP by total primary energy use, can be more than four times as large as the energy productivity β_Y implied by the E3S2 model. This shows that in order to generate GDP trajectories comparable to the SSPs, non-linear dynamics of energy productivity β_Y need to be assumed that lie outside of the support of historical data.

6.2.3 Trends of renewable energy and energy productivity implied in SSP GDP projections

In this section, we examine the necessary growth rates in renewable energy R_t and energy productivity β_Y , respectively, that would be required to achieve the GDP growth implied in the SSP scenarios from 2020 to 2100. This analysis is based on the assumption that all other factors will

Table 6.2: Comparison of d_R (Panel A) and d_{β_Y} (Panel B) implied by SSP 1.9 GDP projections with estimates from historical data. Standard errors are reported in parentheses. If R_t^* or β_Y admits a stochastic trend $d_{R,t}$, the values reported for the historical period are the medians of the smoothed $d_{R,t}$ from 2015 to 2019.

A. estimates of d_R (unit: mtoe yr⁻¹)						
	LAM	REF	OECD	ASIA	MAF	WORLD
SSP1-1.9	47.701 (5.679)	17.275 (9.959)	41.855 (6.634)	130.303 (83.694)	382.815 (61.499)	58.666 (14.49)
SSP2-1.9	51.34 (0.598)	24.574 (5.333)	47.629 (5.679)	85.363 (11.175)	340.03 (74.721)	61.079 (3.49)
SSP5-1.9	76.689 (6.199)	25.894 (8.196)	221.723 (8.169)	276.818 (92.381)	660.879 (129.291)	133.494 (62.583)
historical period	3.164 (0.385)	0.035 (0.197)	16.35 (2.741)	32.289 (1.640)	7.485 (0.382)	60.45 (4.528)
B. estimates of d_{β_Y} (unit: billion USD 2005 (PPP) /mtoe yr⁻¹)						
	LAM	REF	OECD	ASIA	MAF	WORLD
SSP1-1.9	0.483 (0.012)	0.161 (0.007)	0.256 (0.011)	0.485 (0.027)	0.519 (0.054)	0.399 (0.013)
SSP2-1.9	0.043 (0.012)	0.169 (0.031)	0.191 (0.006)	0.23 (0.006)	0.299 (0.013)	0.192 (0.003)
SSP5-1.9	0.189 (0.024)	0.175 (0.053)	0.269 (0.007)	0.433 (0.024)	0.439 (0.057)	0.331 (0.008)
historical period	0.020 (0.020)	0.029 (0.0001)	0.108 (0.011)	0.106 (0.0032)	-0.061 (0.036)	0.103 (0.0015)

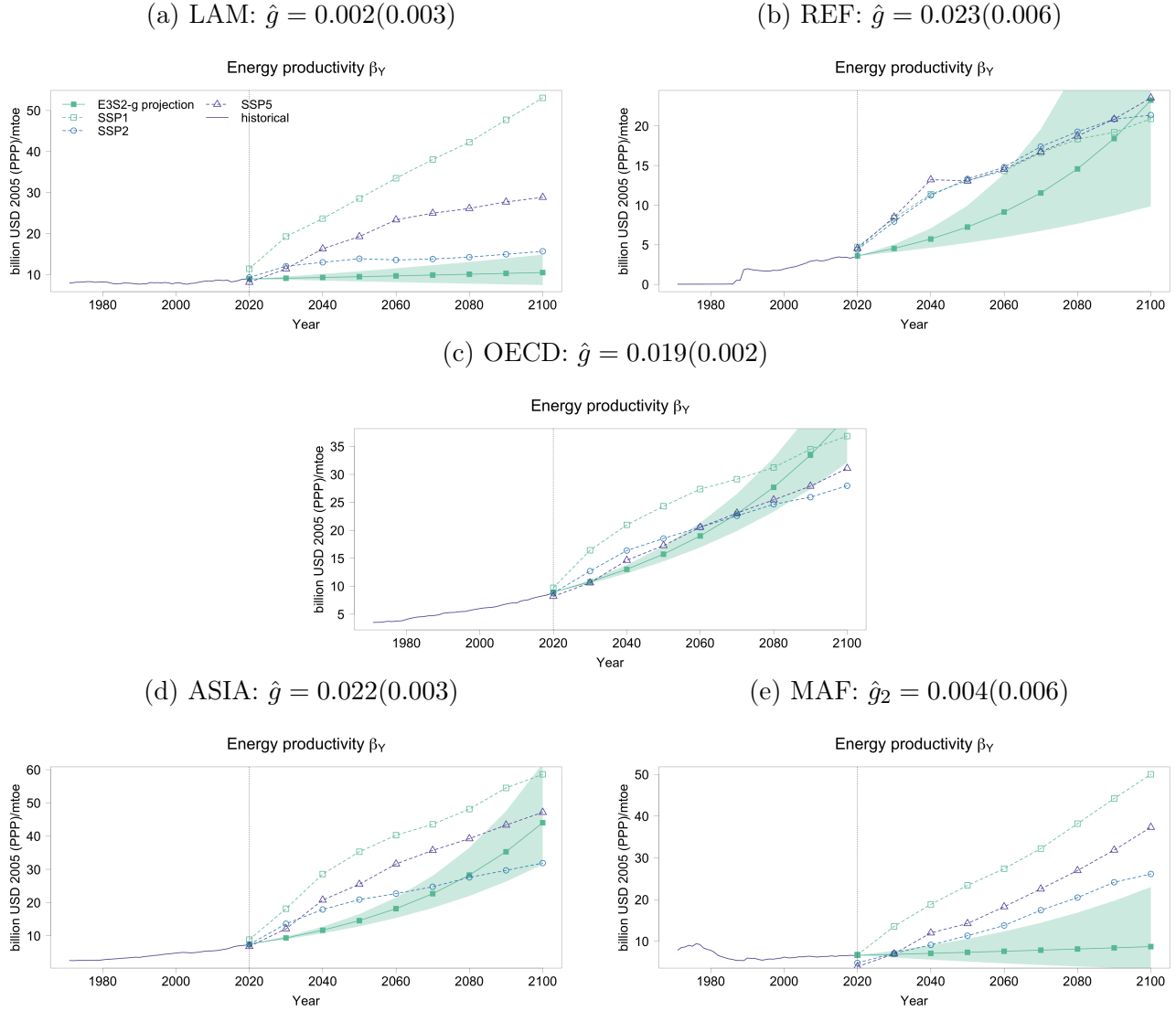
remain the same. We set the emission conversion factors equal to their estimated values. In case of time-varying emission conversion factors, we set them constantly equal to their smoothed value in 2019.

In the first analysis, we only vary R_t , meaning we assume constant energy productivity, and all reductions in fossil sources have to be compensated by growth in renewables. We insert the estimated d_{β_Y} reported in Table 5.1 as the linear trend for β_Y in the future. If β_Y is specified as a local linear trend model, we use the median of the smoothed $d_{\beta_Y,t}$ over the period 2015 – 2019. We assume that all other energy sources follow the trajectories in SSP 1.9. We assume a linear trend d_R for R_t^* and estimate it on the SSP 1.9 data.

In the second analysis, we assume that all energy sources, including renewables, follow the pathways in SSP 1.9. Economic growth is obtained by linear energy productivity improvements brought by technological advancements. Assuming $\sigma_{\beta_Y}^2 = 0$ in Equation 2.5, we estimate the linear trend d_{β_Y} of β_Y on the SSP data.

Table 6.2 shows the estimates from the two analyses and compares with the estimates from the historical period. The table shows that the growth implied by the SSPs in either R_t or $\beta_{Y,t}$ largely exceeds the data estimates, the only exception being the ASIA region.

Figure 6.5: Comparison of β_Y projected by the E3S2-g model and β_Y implied by SSP 1.9 projections. The title of each panel reports the region and growth rate used for projection, which is estimated using historical data. The standard errors are reported in parentheses. \hat{g}_2 in MAF represents the growth rate estimated for the second stage starting from 1990. Confidence bands are pointwise at the 90% level.



6.2.4 Projections with geometric growth in energy productivity

Motivated by the large discrepancies of GDP trajectories from SSPs when assuming linear growth in energy productivity, in this section we consider a variant of the E3S2 model that admits geometric growth in β_Y (E3S2-g model). We model the logarithm of β_Y as the state variable and specify $\log \beta_Y$ as:

$$\log \beta_{Y,t} = g + \log \beta_{Y,t-1} + \eta_{\beta_Y,t-1}. \quad (6.1)$$

6.3 Global scenario analysis

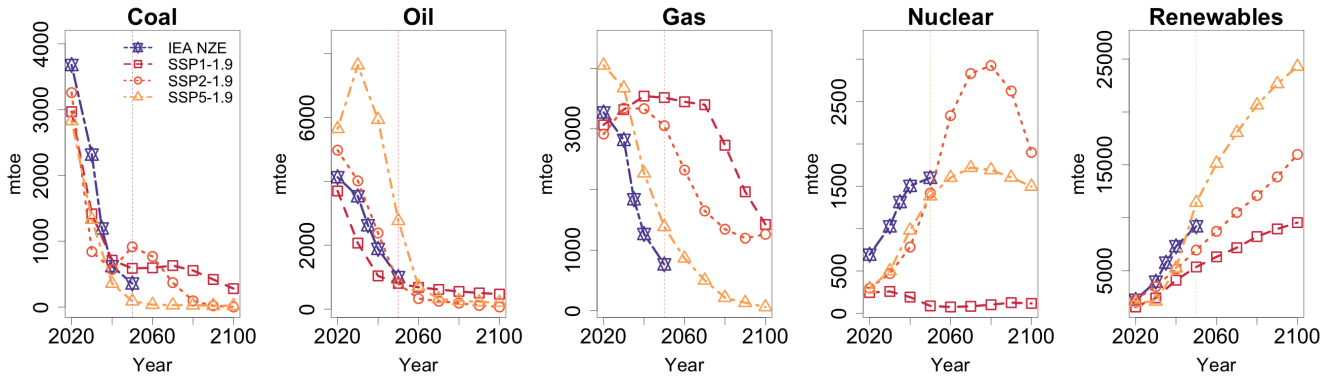
Equation (6.1) specifies $\log \beta_{Y,t} - \log \beta_{Y,t-1}$ as the growth rate g plus an error term $\eta_{\beta,t}$. To simplify the numerical optimization, we set all emission conversion factors as time-invariant and instead introduce an AR(1) structure in the measurement error process to account for autocorrelation. We also set $R_t^* = R_t$ and thus treat renewables as exogenous. The matrix form of the E3S2-g model is presented in Appendix D.1. The energy productivity β_Y of MAF shows a two-stage pattern, whereby β_Y declines in the first two decades, followed by a steady rise since the 1990s. In order to avoid distortions from using a single geometric growth rate to capture this pattern, we estimate the growth rates of these two stages separately. We use the estimate of the second growth rate in the projection. We use the gradient-based algorithm “Limited-memory Broyden-Fletcher-Goldfarb-Shanno with Bound constraints” (L-BFGS-B) (Byrd et al., 1995) embedded in the R function “optim” to maximize the log-likelihood, which performs more stably in the geometric growth specification when compared to the “Nelder-Mead” method.

Figure 6.5 shows that when the energy productivity β_Y is assumed to grow geometrically, three out of the five regions (REF, OECD, and ASIA) have comparable β_Y projections to the SSPs. For the regions LAM and MAF, the E3S2-g model still undershoots by a large margin due to low estimated growth rates g . Detailed results from the E3S2-g model are presented in Appendix D.2, D.3, and D.4, which report parameter estimates, diagnostic statistics, and projections comparison, respectively.

6.3 Global scenario analysis

In this section, we study projections at a global level. Apart from the SSP 1.9 Wm^{-2} scenario we describe in the regional analysis, we also consider an alternative scenario, the IEA Net Zero road map (IEA NZE) (Cozzi et al., 2021).

Figure 6.6: Comparison between global total energy supply pathways of the primary energy sources in the NZE scenario over the period 2020 – 2050 and global SSP 1.9 Wm^{-2} energy trajectories over the period 2020 – 2100. NZE projections are available in 2020, 2030, 2035, 2040, and 2050, while the SSP trajectories provide data at a 10-year frequency from 2020 to 2100.



IEA NZE explores the transition at the global level to a net zero emission energy system by 2050 while adopting a cost-effective pathway and maintaining robust economic growth. It provides

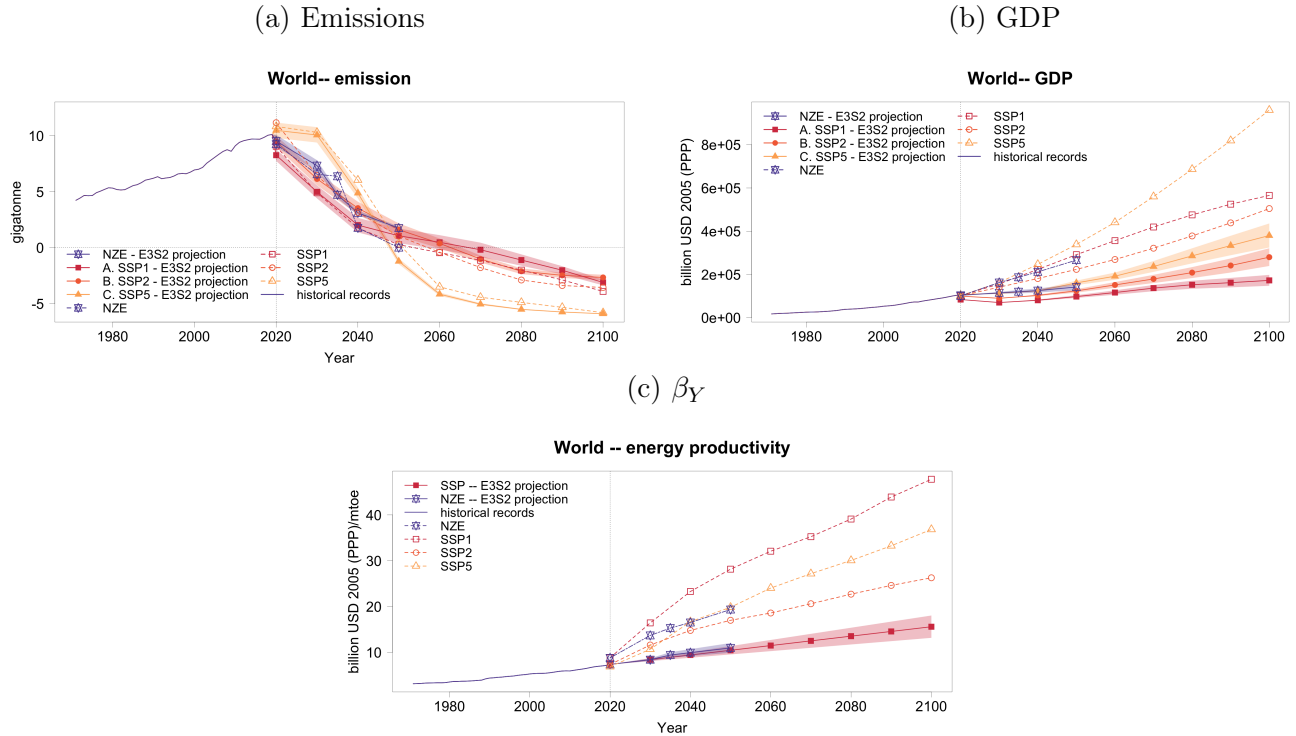
an alternative to SSP 1.9 Wm^{-2} in limiting global mean temperature rise to $1.5^{\circ}C$. Figure 6.6 compares the pathways of the five primary energy sources from SSP 1.9 Wm^{-2} and IEA NZE. Figure 6.6 shows that IEA NZE trajectories are most comparable to SSP5-1.9 in magnitude and variation pattern for coal, gas, nuclear, and renewables, while for oil, it is closer to SSP2-1.9.

We use the parameter estimates from fitting the E3S2 model to global data (Section 5) and adopt the same methodology for constructing projections introduced in Section 6.1. Figure 6.7 compares the long-term projections for CO_2 emissions, GDP, and β_Y from our model, conditional on the energy pathways from SSP 1.9 Wm^{-2} and IEA NZE. GDP projections from IEA NZE are in billion 2022 USD (PPP). We harmonize the series so that the value in 2020 matches the historical value, which is in USD 2005 billion (PPP), so that the NZE values can be compared to the historical dataset in this paper and the SSP values.

Similar to the regional analysis, our model-generated CO_2 emissions projections are comparable to those provided by the scenarios. Up to 2030, the projection series from IEA NZE closely aligns with SSP2-1.9. However, beyond 2030, its decreasing trend accelerates, reaching net zero emissions in 2050. This is earlier than SSP1-1.9 and SSP2-1.9, but slightly later than SSP5-1.9.

The projected GDP and energy productivity (β_Y) from the E3S2 model once again exhibit significantly lower values compared to the corresponding projections from IEA NZE and SSP. The IEA NZE projection is most consistent with SSP1-1.9 in GDP projections and SSP5-1.9 in β_Y projections.

Figure 6.7: Comparison of global projections of CO_2 emission, GDP, and β_Y generated from the E3S2 model and the trajectories from SSP 1.9 Wm^{-2} and IEA NZE scenarios. Confidence bands are pointwise at the 90% level.

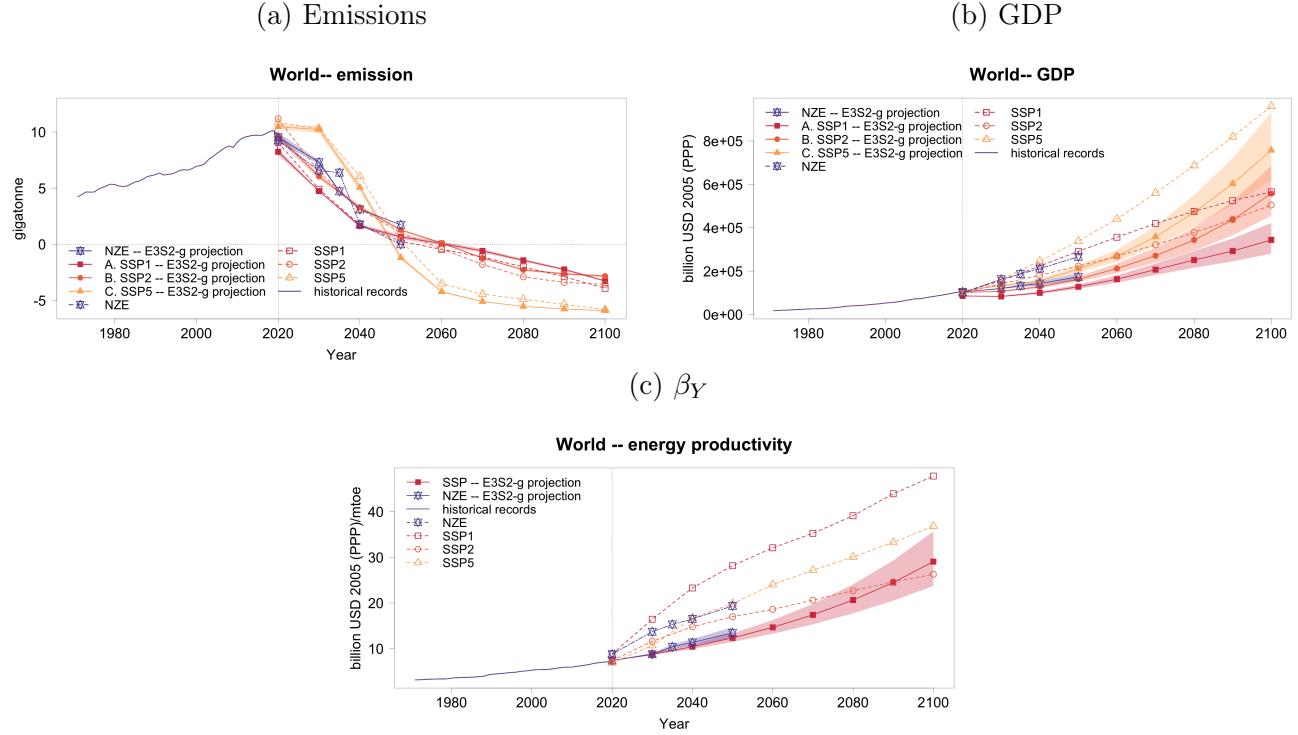


Furthermore, we conduct an estimation and projection using the E3S2-g model based on global-

6.3 Global scenario analysis

level data to compare the geometric growth path with the projected trajectories from SSP1-1.9 and IEA NZE. Detailed parameter estimates and diagnostic statistics from this analysis are provided in Appendix D.2 and D.3, respectively, alongside regional results. The comparative analysis of projections for emissions, GDP, and β_Y is presented in Figure 6.8.

Figure 6.8: Comparison of global projections of CO₂ emission, GDP, and β_Y generated from the E3S2-g model and the trajectories from SSP 1.9 Wm⁻² and IEA NZE scenarios. Confidence bands are pointwise at the 90% level.



A comparison of Panel (a) in Figure 6.7 and Figure 6.8 highlights a notable resemblance between the projection medians. This similarity is expected, given that the specification of geometric growth primarily influence GDP and β_Y projections. Nevertheless, the linear trend projection presented in Panel (a) of 6.7 exhibits slightly wider confidence bands, due to larger uncertainty estimates.

Under geometric growth, the projections for GDP and energy productivity show considerable increases, more than doubling the values projected under a linear growth assumption. The trajectory of GDP generated by the E3S2-g model, when conditional on SSP2-1.9, aligns with the path from the SSP assessment. However, in the two other SSP 1.9 scenarios, the paths generated by the E3S2-g model still fall short of the SSP counterparts.

7 Conclusion

In this paper, we present a non-linear Gaussian state space system for CO₂ emissions, GDP, and the energy mix (E3S2 model). The E3S2 model consists of three modules: energy, emissions, and economy. The energy module takes the consumption quantities of coal, oil, gas, and nuclear energy as exogenously given and models a deterministic or stochastic trend in renewable energy. The emission module represents CO₂ emissions as a weighted linear combination of fossil fuels, where we allow the weights, i.e., the emission conversion factors, to vary over time. The economy module specifies GDP as the product of the energy productivity β_Y and the aggregate of the consumption quantities of the five primary energy sources.

The E3S2 model is a general form nesting many specifications. It is a flexible statistical model capable of capturing time-varying dynamics, addressing non-stationarity, and assessing estimation and projection uncertainty. It can be adapted to data from various geographic resolutions, including regions or countries.

We follow a data-driven model selection procedure to choose an appropriate form for global analysis and the five regions considered in the SSP scenarios. The E3S2 model is estimated using maximum likelihood via the extended Kalman filter. We find that most of our emission conversion factor estimates are in line with benchmarks in the literature, especially when we take estimation uncertainty into consideration. Worldwide, and for the two regions MAF and LAM, the emission conversion factor of coal has been declining over time, while for OECD, it is gas that shows a downward trend.

We perform long-term projections conditional on the fuel mix pathways from SSP 1.9 Wm^{-2} scenarios and the IEA Net Zero by 2050 roadmap. The emissions projections align with those from these two scenarios. This shows that the emission conversion factors estimated by the E3S2 model are consistent with those used in the SSP and IEA-NZE projections.

However, our GDP projections, constructed on the assumption of a linear trend in energy productivity, present a much less optimistic picture. In an alternative specification (E3S2-g model), where energy productivity has geometric growth, the GDP projections align better. For the three regions OECD, ASIA, and REF, the GDP projections from the E3S2-g model are compatible with the trajectories outlined in SSP 1.9, although they still fall short.

Our results indicate that following the economic growth paths of SSP and IEA-NZE trajectories necessitates rapid growth trajectories for the energy productivity factor β_Y , deviating considerably from historical trends. If the green transition is to align in terms of GDP growth with the scenarios set forth in SSPs and by the IEA, drastic and transformative change in energy intensity of GDP is necessary.

References

- Adedoyin, F. F., Ozturk, I., Bekun, F. V., Agboola, P. O., & Agboola, M. O. (2021). Renewable and non-renewable energy policy simulations for abating emissions in a complex economy: evidence from the novel dynamic ARDL. *Renewable Energy*, 177, 1408–1420.
- Apergis, N., & Payne, J. E. (2009). CO2 emissions, energy usage, and output in Central America. *Energy Policy*, 37(8), 3282–3286.
- Bennedsen, M., Hillebrand, E., & Jensen, S. (2023). A neural network approach to the environmental Kuznets curve. *Energy Economics*, 126, 106985.
- Bennedsen, M., Hillebrand, E., & Koopman, S. J. (2023). A multivariate dynamic statistical model of the global carbon budget 1959–2020. *Journal of the Royal Statistical Society Series A: Statistics in Society*, 186(1), 20–42.
- Box, G. E., & Pierce, D. A. (1970). Distribution of residual autocorrelations in autoregressive-integrated moving average time series models. *Journal of the American Statistical Association*, 65(332), 1509–1526.
- Byrd, R. H., Lu, P., Nocedal, J., & Zhu, C. (1995). A limited memory algorithm for bound constrained optimization. *SIAM Journal on scientific computing*, 16(5), 1190–1208.
- Caines, P. (1988). *Linear Stochastic Systems*. Wiley.
- Calvin, K., Bond-Lamberty, B., Clarke, L., Edmonds, J., Eom, J., Hartin, C., . . . Moss, R. (2017). The SSP4: A world of deepening inequality. *Global Environmental Change*, 42, 284–296.
- Castle, J., & Hendry, D. F. (2020). Climate econometrics: An overview. *Foundations and Trends in Econometrics*, 10(3-4), 145–322.
- Cozzi, L., Gül, T., Bouckaert, S., Pales, A. F., McGlade, C., Remme, U., . . . Spencer, T. (2021). *Net zero by 2050: A roadmap for the global energy sector* (Tech. Rep.). Paris: International Energy Agency.
- Cozzi, L., Wetzels, D., & Bouckaert, S. (2022). *Africa energy outlook 2022* (Tech. Rep.). Paris: International Energy Agency.
- Creutzig, F., Ravindranath, N. H., Berndes, G., Bolwig, S., Bright, R., Cherubini, F., . . . Faaij, A. (2015). Bioenergy and climate change mitigation: an assessment. *GCB Bioenergy*, 7(5), 916–944.
- Crost, B., & Traeger, C. P. (2013). Optimal climate policy: uncertainty versus Monte Carlo. *Economics Letters*, 120(3), 552–558.
- Csereklyei, Z., & Stern, D. I. (2015). Global energy use: Decoupling or convergence? *Energy Economics*, 51, 633–641.
- Cuaresma, J. C. (2017). Income projections for climate change research: A framework based on human capital dynamics. *Global Environmental Change*, 42, 226–236.
- Dellink, R., Chateau, J., Lanzi, E., & Magné, B. (2017). Long-term economic growth projections in the Shared Socioeconomic Pathways. *Global Environmental Change*, 42, 200–214.
- Durbin, J., & Koopman, S. J. (2012). *Time series analysis by state space methods* (Revised ed.).

Oxford University Press.

- Emmerling, J., Drouet, L., Reis, L., Bevione, M., Berger, L., Bosetti, V., ... Longden, T. (2016). *The WITCH 2016 model-documentation and implementation of the shared socioeconomic pathways* (Tech. Rep. No. 42.2016). Venice: Fondazione Eni Enrico Mattei Research Paper.
- Fricko, O., Havlik, P., Rogelj, J., Klimont, Z., Gusti, M., Johnson, N., ... Amann, M. (2017). The marker quantification of the Shared Socioeconomic Pathway 2: A middle-of-the-road scenario for the 21st century. *Global Environmental Change*, 42, 251–267.
- Friedlingstein, P., O’sullivan, M., Jones, M. W., Andrew, R. M., Gregor, L., Hauck, J., ... Peters, G. P. (2022). Global Carbon Budget 2022. *Earth System Science Data*, 14(11), 4811–4900.
- Fujimori, S., Hasegawa, T., Masui, T., Takahashi, K., Herran, D. S., Dai, H., ... Kainuma, M. (2017). SSP3: AIM implementation of Shared Socioeconomic Pathways. *Global Environmental Change*, 42, 268–283.
- Grossman, G. M., & Krueger, A. B. (1991). *Environmental Impacts of a North American Free Trade Agreement* (Working Paper No. 3914). National Bureau of Economic Research. Retrieved from <http://www.nber.org/papers/w3914> doi: 10.3386/w3914
- Hamakawa, Y. (2004). Background and motivation for thin-film solar-cell development. In *Thin-film solar cells: Next generation photovoltaics and its applications* (pp. 1–14). Springer.
- Hamit-Haggar, M. (2012). Greenhouse gas emissions, energy consumption and economic growth: A panel cointegration analysis from canadian industrial sector perspective. *Energy Economics*, 34(1), 358–364.
- Hong, B., & Slatick, E. (1994). Carbon dioxide emission factors for coal. In Energy Information Administration (Ed.), *Quarterly coal report, Jan-Mar 1994*.
- Jarque, C. M., & Bera, A. K. (1980). Efficient tests for normality, homoscedasticity and serial independence of regression residuals. *Economics Letters*, 6(3), 255–259.
- Kriegler, E., Bauer, N., Popp, A., Humpenöder, F., Leimbach, M., Strefler, J., ... Klein, D. (2017). Fossil-fueled development (SSP5): An energy and resource intensive scenario for the 21st century. *Global Environmental Change*, 42, 297–315.
- Leimbach, M., Kriegler, E., Roming, N., & Schwanitz, J. (2017). Future growth patterns of world regions—A GDP scenario approach. *Global Environmental Change*, 42, 215–225.
- Leitão, J., Ferreira, J., & Santibanez-González, E. (2022). New insights into decoupling economic growth, technological progress and carbon dioxide emissions: Evidence from 40 countries. *Technological Forecasting and Social Change*, 174, 121250.
- Ljung, G. M., & Box, G. E. (1978). On a measure of lack of fit in time series models. *Biometrika*, 65(2), 297–303.
- Lu, W.-C. (2017). Greenhouse gas emissions, energy consumption and economic growth: a panel cointegration analysis for 16 Asian countries. *International Journal of Environmental Research and Public Health*, 14(11), 1436.
- Mangino, J., Mareckova, K., Pulles, T., & Tanabe, K. (2002). *Establishment of the Intergovernmental Panel on Climate Change (IPCC) Emission Factor Database* (Tech. Rep.). Intergovern-

- mental Panel on Climate Change. Retrieved from <https://www.ipcc-nggip.iges.or.jp/EFDB/main.php>
- Markovic, M., Garijo, D., Germano, S., & Naja, I. (2023). TEC: Transparent emissions calculation toolkit. In T. R. Payne et al. (Eds.), *The semantic web – iswc 2023* (pp. 76–93). Springer Nature.
- Marland, G., & Rotty, R. M. (1984). Carbon dioxide emissions from fossil fuels: a procedure for estimation and results for 1950–1982. *Tellus B: Chemical and Physical Meteorology*, 36(4), 232–261.
- Mitić, P., Fedajev, A., Radulescu, M., & Rehman, A. (2023). The relationship between CO2 emissions, economic growth, available energy, and employment in SEE countries. *Environmental Science and Pollution Research*, 30(6), 16140–16155.
- Nelder, J. A., & Mead, R. (1965). A simplex method for function minimization. *The Computer Journal*, 7(4), 308–313.
- Nordhaus, W. (2018). Evolution of modeling of the economics of global warming: changes in the DICE model, 1992–2017. *Climatic change*, 148(4), 623–640.
- Omara, M., Zavala-Araiza, D., Lyon, D. R., Hmiel, B., Roberts, K. A., & Hamburg, S. P. (2022). Methane emissions from us low production oil and natural gas well sites. *Nature Communications*, 13(1), 2085.
- Pao, H.-T., & Tsai, C.-M. (2010). CO2 emissions, energy consumption and economic growth in BRIC countries. *Energy Policy*, 38(12), 7850–7860.
- Parrique, T., Barth, J., Briens, F., Kerschner, C., Kraus-Polk, A., Kuokkanen, A., & Spangenberg, J. H. (2019). *Decoupling debunked: Evidence and arguments against green growth as a sole strategy for sustainability* (Tech. Rep.). Brussels: European Environment Bureau.
- Riahi, K., van Vuuren, D. P., Kriegler, E., Edmonds, J., O'Neill, B. C., Fujimori, S., ... Tavoni, M. (2017). The Shared Socioeconomic Pathways and their energy, land use, and greenhouse gas emissions implications: An overview. *Global Environmental Change*, 42, 153–168. doi: 10.1016/j.gloenvcha.2016.05.009
- Rogelj, J., Popp, A., Calvin, K. V., Luderer, G., Emmerling, J., Gernaat, D., ... Marangoni, G. (2018). Scenarios towards limiting global mean temperature increase below 1.5 °C. *Nature Climate Change*, 8(4), 325–332.
- Roten, D., Marland, G., Bun, R., Crippa, M., Gilfillan, D., Jones, M. W., ... Andrew, R. (2022). CO2 emissions from energy systems and industrial processes: Inventories from data-and proxy-driven approaches. In B. Poulter, J. G. Canadell, D. J. Hayes, & R. L. Thompson (Eds.), *Balancing greenhouse gas budgets* (pp. 31–57). Elsevier.
- Schurr, S., & Netschert, B. (1960). *Energy and the American Economy, 1850–1975*. Johns Hopkins University Press.
- Shephard, N. (1993). Distribution of the ML estimator of an MA (1) and a local level model. *Econometric Theory*, 9(3), 377–401.
- Stern, D. I. (2004a). Economic growth and energy. *Encyclopedia of Energy*, 2(147), 35–51.

- Stern, D. I. (2004b). The rise and fall of the environmental Kuznets curve. *World Development*, 32(8), 1419–1439.
- United Nations. (2015). *Transforming our world: the 2030 Agenda for Sustainable Development* (Tech. Rep.). New York: Author.
- Van Vuuren, D. P., Stehfest, E., Gernaat, D. E., Doelman, J. C., Van den Berg, M., Harmsen, M., ... Edelenbosch, O. Y. (2017). Energy, land-use and greenhouse gas emissions trajectories under a green growth paradigm. *Global Environmental Change*, 42, 237–250.
- Yue, X.-G., Liao, Y., Zheng, S., Shao, X., & Gao, J. (2021). The role of green innovation and tourism towards carbon neutrality in Thailand: Evidence from bootstrap ADRL approach. *Journal of Environmental Management*, 292, 112778.
- Zoundi, Z. (2017). CO2 emissions, renewable energy and the environmental Kuznets curve, a panel cointegration approach. *Renewable and Sustainable Energy Reviews*, 72, 1067–1075.

Appendix

A List of countries included in SSP regions but excluded in our analysis

- The five regions defined by the SSPs contain 190 countries, whereas our dataset contains 146 countries (primarily limited by the coverage of the IEA energy data). The 44 countries included in SSP regions but absent in our dataset are:

OECD: Guam, Puerto Rico;

ASIA: Afghanistan, Bhutan, Fiji, French Polynesia, Maldives, Federated States of Micronesia, New Caledonia, Papua New Guinea, Samoa, Solomon Islands, Timor-Leste, Vanuatu;

MAF: Burkina Faso, Burundi, Cape Verde, Central African Republic, Chad, Comoros, Djibouti, Gambia, Guinea, Guinea-Bissau, Lesotho, Liberia, Malawi, Mali, Mauritania, Mayotte, Occupied Palestinian Territory, Réunion, Sierra Leone, Somalia, Western Sahara;

LAM: Aruba, Bahamas, Barbados, Belize, French Guiana, Grenada, Guadeloupe, Martinique, Virgin Islands (US).

B The matrix form of the E3S2 model

The matrix form of a non-linear Gaussian state space model can be written as ([Durbin & Koopman, 2012](#)),

$$\begin{aligned}\mathbf{X}_t &= \mathbf{T}_{t-1}(\mathbf{X}_{t-1}) + \mathbf{R}_{t-1}(\mathbf{X}_{t-1}) \boldsymbol{\eta}_{t-1} \\ \mathbf{Y}_t &= \mathbf{Z}_t(\mathbf{X}_t) + \boldsymbol{\varepsilon}_t,\end{aligned}\tag{B.1}$$

where \mathbf{X}_t , \mathbf{Y}_t , $\boldsymbol{\eta}_{t-1}$, and $\boldsymbol{\varepsilon}_t$ denote vectors of state variables, observations, state disturbances, and measurement errors, respectively. The transition matrices $\mathbf{T}_{t-1}(\mathbf{X}_{t-1})$, $\mathbf{R}_{t-1}(\mathbf{X}_{t-1})$, and $\mathbf{Z}_t(\mathbf{X}_t)$ are functions of state variables. Expanding these matrix functions in Taylor series and neglecting the higher-order terms, Equation (B.1) can be linearized as:

$$\begin{aligned}\mathbf{X}_t &= \dot{\mathbf{T}}_{t-1} \mathbf{X}_{t-1} + \mathbf{c}_{t-1} + \mathbf{R}_{t-1}(\mathbf{x}_{t-1|t-1}) \boldsymbol{\eta}_{t-1} \\ \mathbf{Y}_t &= \dot{\mathbf{Z}}_t \mathbf{X}_t + \mathbf{d}_t + \boldsymbol{\varepsilon}_t,\end{aligned}\tag{B.2}$$

where

$$\begin{aligned}\dot{\mathbf{Z}}_t &= \left. \frac{\partial \mathbf{Z}_t(\mathbf{X}_t)}{\partial \mathbf{X}_t'} \right|_{\mathbf{X}_t=\mathbf{x}_t}, \quad \dot{\mathbf{T}}_{t-1} = \left. \frac{\partial \mathbf{T}_{t-1}(\mathbf{X}_{t-1})}{\partial \mathbf{X}_{t-1}'} \right|_{\mathbf{X}_{t-1}=\mathbf{x}_{t-1|t-1}}, \\ \mathbf{d}_t &= \mathbf{Z}_t(\mathbf{x}_t) - \dot{\mathbf{Z}}_t \mathbf{x}_t, \quad \mathbf{c}_{t-1} = \mathbf{T}_{t-1}(\mathbf{x}_{t-1|t-1}) - \dot{\mathbf{T}}_{t-1} \mathbf{x}_{t-1|t-1}, \\ \boldsymbol{\eta}_{t-1} &\sim (\mathbf{0}, \mathbf{Q}_{t-1}(\mathbf{x}_{t-1|t-1})), \quad \boldsymbol{\varepsilon}_t \sim (\mathbf{0}, \mathbf{H}_t(\mathbf{x}_t)),\end{aligned}\tag{B.3}$$

and

$$\mathbf{x}_t = \mathbb{E}(\mathbf{X}_t \mid \mathbf{X}_{t-1}), \quad \mathbf{x}_{t|t} = \mathbb{E}(\mathbf{X}_t \mid \mathbf{Y}_t). \quad (\text{B.4})$$

In the E3S2 model, the state equations are

$$\underbrace{\begin{pmatrix} E_t^* \\ Y_t^* \\ \beta_{C,t} \\ \beta_{O,t} \\ \beta_{G,t} \\ \beta_{Y,t} \\ R_t^* \\ d_{R,t} \\ d_{\beta_Y,t} \end{pmatrix}}_{\mathbf{x}_t} = \underbrace{\begin{pmatrix} \beta_{C,t-1}C_t + \beta_{O,t-1}O_t + \beta_{G,t-1}G_t \\ \beta_{Y,t-1}(C_t + O_t + G_t + N_t + d_{R,t-1} + R_{t-1}^*) \\ \beta_{C,t-1} \\ \beta_{O,t-1} \\ \beta_{G,t-1} \\ d_{\beta_Y,t-1} + \beta_{Y,t-1} \\ d_{R,t-1} + R_{t-1} \\ d_{R,t-1} \\ d_{\beta_Y,t-1} \end{pmatrix}}_{\mathbf{T}_{t-1}(\mathbf{x}_{t-1})} + \underbrace{\begin{pmatrix} 1 & 0 & C_t & O_t & G_t & 0 & 0 & 0 & 0 \\ 0 & 1 & 0 & 0 & 0 & 0 & \beta_{Y,t-1|t-1} & 0 & 0 \\ 0 & 0 & 1 & 0 & 0 & 0 & 0 & 0 & 0 \\ 0 & 0 & 0 & 1 & 0 & 0 & 0 & 0 & 0 \\ 0 & 0 & 0 & 0 & 1 & 0 & 0 & 0 & 0 \\ 0 & 0 & 0 & 0 & 0 & 1 & 0 & 0 & 0 \\ 0 & 0 & 0 & 0 & 0 & 0 & 1 & 0 & 0 \\ 0 & 0 & 0 & 0 & 0 & 0 & 0 & 1 & 0 \\ 0 & 0 & 0 & 0 & 0 & 0 & 0 & 0 & 1 \end{pmatrix}}_{\mathbf{R}_{t-1|t-1}(\mathbf{x}_{t-1|t-1})} \underbrace{\begin{pmatrix} \eta_{E,t-1} \\ \eta_{Y,t-1} \\ \eta_{\beta_C,t-1} \\ \eta_{\beta_O,t-1} \\ \eta_{\beta_G,t-1} \\ \eta_{\beta_Y,t-1} \\ \eta_{R,t-1} \\ \eta_{d_R,t-1} \\ \eta_{d_{\beta_Y,t-1}} \end{pmatrix}}_{\boldsymbol{\eta}_{t-1}}, \quad (\text{B.5})$$

and the measurement equations are

$$\underbrace{\begin{pmatrix} E_t \\ Y_t \\ R_t \end{pmatrix}}_{\mathbf{Y}_t} = \underbrace{\begin{pmatrix} E_t^* \\ Y_t^* \\ R_t^* \end{pmatrix}}_{\mathbf{Z}_t(\mathbf{x}_t)} + \underbrace{\begin{pmatrix} \varepsilon_t^E \\ \varepsilon_t^Y \\ \varepsilon_t^R \end{pmatrix}}_{\boldsymbol{\varepsilon}_t}. \quad (\text{B.6})$$

The Jacobian matrix in Equation (B.3) takes the form:

$$\dot{\mathbf{T}}_{t-1} = \begin{pmatrix} 0 & 0 & C_t & O_t & G_t & 0 & 0 & 0 & 0 \\ 0 & 0 & 0 & 0 & 0 & h_{t-1|t-1} & \beta_{Y,t-1|t-1} & \beta_{Y,t-1|t-1} & \beta_{Y,t-1|t-1} \\ 0 & 0 & 1 & 0 & 0 & 0 & 0 & 0 & 0 \\ 0 & 0 & 0 & 1 & 0 & 0 & 0 & 0 & 0 \\ 0 & 0 & 0 & 0 & 1 & 0 & 0 & 0 & 0 \\ 0 & 0 & 0 & 0 & 0 & 1 & 0 & 0 & 1 \\ 0 & 0 & 0 & 0 & 0 & 0 & 1 & 1 & 0 \\ 0 & 0 & 0 & 0 & 0 & 0 & 0 & 1 & 0 \\ 0 & 0 & 0 & 0 & 0 & 0 & 0 & 0 & 1 \end{pmatrix}, \quad (\text{B.7})$$

where

$$h_{t-1|t-1} = C_t + O_t + G_t + N_t + d_{R,t-1|t-1} + R_{t-1|t-1}^*,$$

and

$$\dot{\mathbf{Z}}_t = \mathbf{Z}(\mathbf{x}_t) = \begin{pmatrix} 1 & 0 & 0 & 0 & 0 & 0 & 0 & 0 & 0 \\ 0 & 1 & 0 & 0 & 0 & 0 & 0 & 0 & 0 \\ 0 & 0 & 0 & 0 & 0 & 0 & 1 & 0 & 0 \end{pmatrix}. \quad (\text{B.8})$$

The variance-covariance matrices of the state disturbances and measurement errors are independent of the state variables:

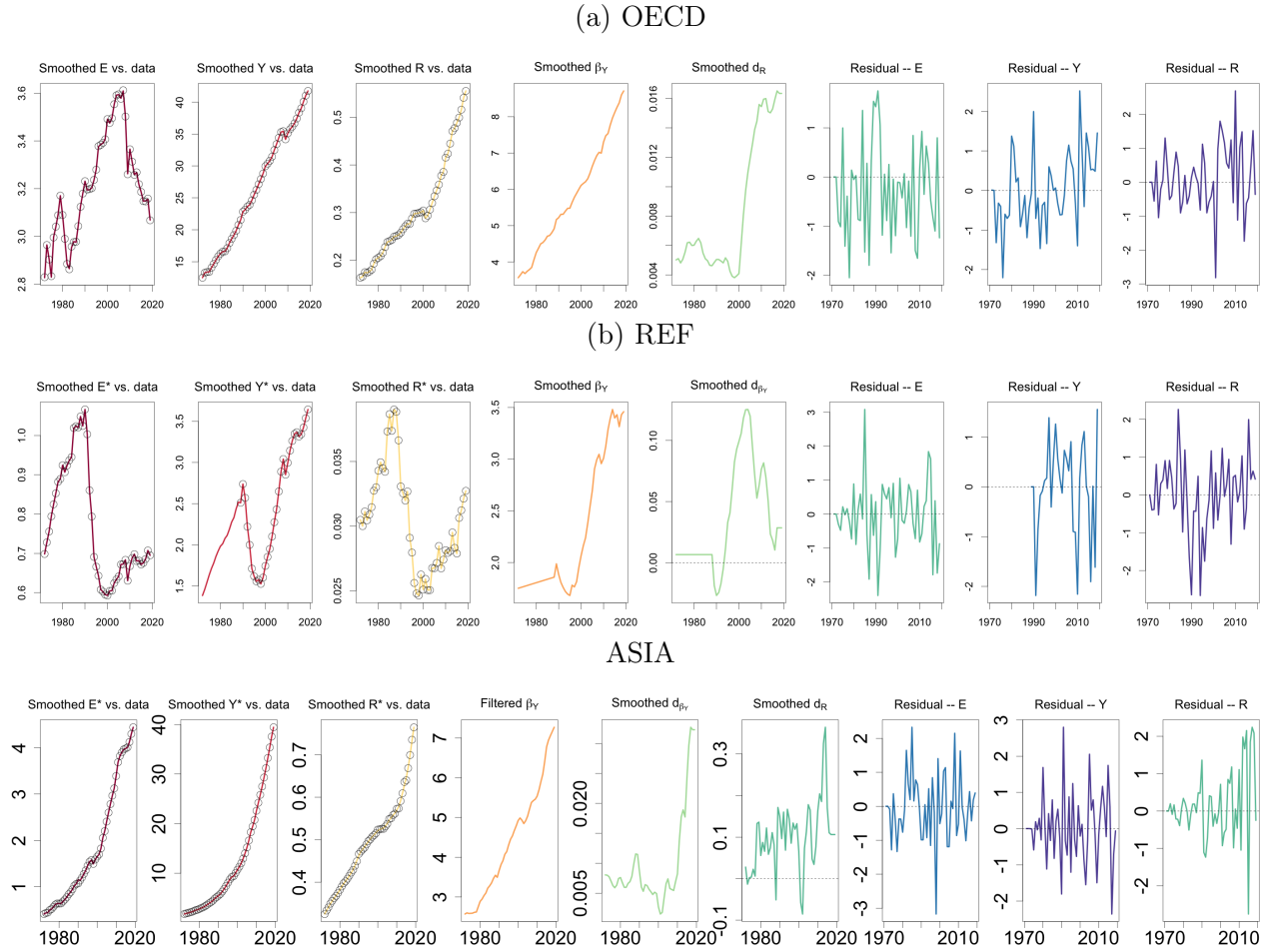
$$\mathbf{Q}_{t-1}(\mathbf{x}_{t-1|t-1}) = \mathbf{Q} = \begin{pmatrix} \sigma_{\eta_E}^2 & 0 & 0 & 0 & 0 & 0 & 0 & 0 & 0 \\ 0 & \sigma_{\eta_Y}^2 & 0 & 0 & 0 & 0 & 0 & 0 & 0 \\ 0 & 0 & \sigma_{\eta_{\beta_C}}^2 & 0 & 0 & 0 & 0 & 0 & 0 \\ 0 & 0 & 0 & \sigma_{\eta_{\beta_O}}^2 & 0 & 0 & 0 & 0 & 0 \\ 0 & 0 & 0 & 0 & \sigma_{\eta_{\beta_G}}^2 & 0 & 0 & 0 & 0 \\ 0 & 0 & 0 & 0 & 0 & \sigma_{\eta_{\beta_Y}}^2 & 0 & 0 & 0 \\ 0 & 0 & 0 & 0 & 0 & 0 & \sigma_{\eta_R}^2 & 0 & 0 \\ 0 & 0 & 0 & 0 & 0 & 0 & 0 & \sigma_{\eta_{d_R}}^2 & 0 \\ 0 & 0 & 0 & 0 & 0 & 0 & 0 & 0 & \sigma_{\eta_{d_{\beta_Y}}}^2 \end{pmatrix} \quad (\text{B.9})$$

and

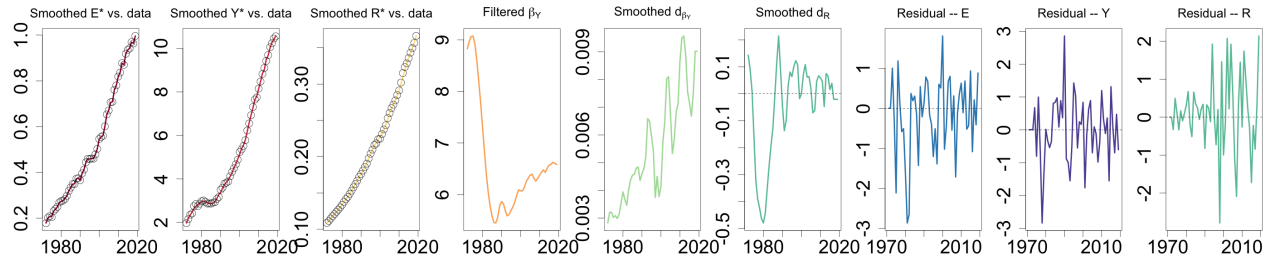
$$\mathbf{H}_t(\mathbf{x}_t) = \mathbf{H} = \begin{pmatrix} \sigma_{\varepsilon_E}^2 & 0 & 0 \\ 0 & \sigma_{\varepsilon_Y}^2 & 0 \\ 0 & 0 & \sigma_{\varepsilon_R}^2 \end{pmatrix}. \quad (\text{B.10})$$

C Further results for the E3S2 model

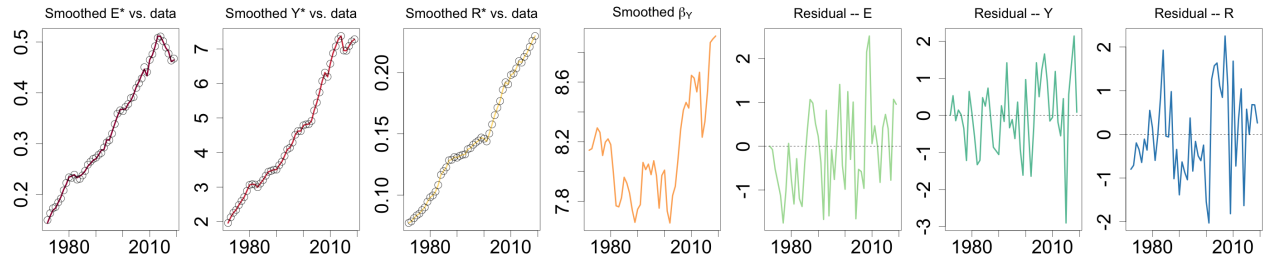
Figure C.1: Smoothed states of E^* , Y^* , and R^* (solid lines) compared to data (circles); smoothed energy productivity β_Y and smoothed stochastic trend of β_Y (if any) and of R^* (if any); residuals (one-step ahead standardized prediction errors of E^* , Y^* , and R^*).



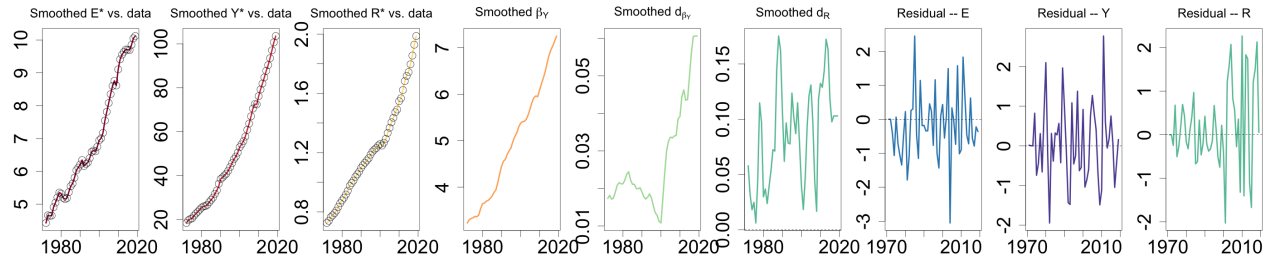
(c) MAF



(d) LAM



(e) WORLD



D E3S2-g model

D.1 The matrix form of the E3S2-g model

State equation:

$$\begin{pmatrix} E_t^* \\ Y_t^* \\ \beta_{C,t} \\ \beta_{O,t} \\ \beta_{G,t} \\ \log \beta_{Y,t} \\ \alpha_t^* \end{pmatrix} = \begin{pmatrix} \beta_{C,t-1}C_t + \beta_{O,t-1}O_t + \beta_{G,t-1}G_t \\ \exp(\log \beta_{Y,t-1})(C_t + O_t + G_t + N_t + R_t) \\ \beta_{C,t-1} \\ \beta_{O,t-1} \\ \beta_{G,t-1} \\ g + \log \beta_{Y,t-1} \\ \phi \alpha_{t-1}^* \end{pmatrix} + \begin{pmatrix} 1 & 0 & C_t & O_t & G_t & 0 & 0 \\ 0 & 1 & 0 & 0 & 0 & 0 & 0 \\ 0 & 0 & 1 & 0 & 0 & 0 & 0 \\ 0 & 0 & 0 & 1 & 0 & 0 & 0 \\ 0 & 0 & 0 & 0 & 1 & 0 & 0 \\ 0 & 0 & 0 & 0 & 0 & 1 & 0 \\ 0 & 0 & 0 & 0 & 0 & 0 & 1 \end{pmatrix} \begin{pmatrix} \eta_{E,t-1} \\ \eta_{Y,t-1} \\ \eta_{\beta_C,t-1} \\ \eta_{\beta_O,t-1} \\ \eta_{\beta_G,t-1} \\ \eta_{\beta_Y,t-1} \\ \eta_{\alpha,t-1} \end{pmatrix}. \quad (\text{D.1})$$

Measurement equation:

$$\begin{pmatrix} E_t \\ Y_t \end{pmatrix} = \begin{pmatrix} E_t^* + \alpha_t^* \\ Y_t^* \end{pmatrix} + \begin{pmatrix} \varepsilon_t^E \\ \varepsilon_t^Y \end{pmatrix}. \quad (\text{D.2})$$

The Jacobian matrix $\dot{\mathbf{T}}_{t-1}$ takes the form:

$$\dot{\mathbf{T}}_{t-1} = \begin{pmatrix} 0 & 0 & C_t & O_t & G_t & 0 & 0 \\ 0 & 0 & 0 & 0 & 0 & \exp(\log \beta_{Y,t-1|t-1})(C_t + O_t + G_t + N_t + R_t) & 0 \\ 0 & 0 & 1 & 0 & 0 & 0 & 0 \\ 0 & 0 & 0 & 1 & 0 & 0 & 0 \\ 0 & 0 & 0 & 0 & 1 & 0 & 0 \\ 0 & 0 & 0 & 0 & 0 & 1 & 0 \\ 0 & 0 & 0 & 0 & 0 & 0 & \phi \end{pmatrix}. \quad (\text{D.3})$$

D.2 Parameter estimates

Table D.1: Point estimates and standard errors (in parentheses) of CO₂ emission conversion factors β_C , β_O , and β_G , of the geometric growth rate g , of the AR(1) coefficient ϕ for the AR term in the measurement equation (for the five regions) or the state equation (for WORLD), and of coefficients of dummies D in the E3S2-g model. The superscript of D refers to whether the dummy is included in the state equation (S) or the measurement equation (M), and the subscript refers to the variable name and time index of the dummy. Emission conversion factors are in the unit of tonne CO₂ equivalent per tonne of oil equivalent (tonne CO₂e/ toe).

	$\hat{\beta}_C$	$\hat{\beta}_O$	$\hat{\beta}_G$	\hat{g}	$\hat{\phi}$		
LAM	2.237 (2.695)	3.318 (0.179)	2.415 (0.246)	0.002 (0.003)	0.586 (0.294)		
	$\hat{\beta}_C$	$\hat{\beta}_O$	$\hat{\beta}_G$	\hat{g}	$\hat{\phi}$	$\hat{D}_{E,2015}^M$	
REF	1.865 (1.282)	3.926 (1.576)	2.566 (0.167)	0.023 (0.006)	0.569 (0.177)	0.025 (0.007)	
	$\hat{\beta}_C$	$\hat{\beta}_O$	$\hat{\beta}_G$	\hat{g}	$\hat{\phi}$	$\hat{D}_{E,1990}^S$	
OECD	4.212 (0.459)	2.768 (0.219)	2.591 (0.103)	0.019 (0.002)	0.815 (0.108)	0.033 (0.010)	
	$\hat{\beta}_C$	$\hat{\beta}_O$	$\hat{\beta}_G$	\hat{g}	$\hat{\phi}$	$\hat{D}_{E,2004}^S$	$\hat{D}_{E,1990}^M$
ASIA	3.815 (0.452)	4.148 (0.785)	0.615 (0.705)	0.022 (0.003)	0.503 (0.132)	-0.075 (0.022)	-0.072 (0.022)
	$\hat{\beta}_C$	$\hat{\beta}_O$	$\hat{\beta}_G$	\hat{g}_1	\hat{g}_2	$\hat{\phi}$	$\hat{D}_{Y,1982}^S$ $\hat{D}_{Y,1990}^M$
MAF	6.132 (18.713)	1.32 (1.018)	3.569 (0.532)	-0.019 (0.007)	0.004 (0.006)	0.979 (0.06)	-0.104 (0.080) 0.212 (0.070)
	$\hat{\beta}_C$	$\hat{\beta}_O$	$\hat{\beta}_G$	\hat{g}	$\hat{\phi}$	$\hat{D}_{E,1991}^S$	$\hat{D}_{Y,1990}^M$ $\hat{D}_{Y,1989}^M$
WORLD	3.788 (0.443)	3.188 (0.127)	2.385 (0.180)	0.017 (0.002)	0.524 (0.122)	0.156 (0.027)	1.086 (0.312) 1.040 (0.296)

D.3 Diagnostics

Table D.2: Diagnostic statistics of the standardized one-step ahead prediction errors of emissions and GDP for the E3S2-g model. It reports the first four moments (mean, standard deviation (Std), skewness (Skew), and kurtosis (Kurt) as well the test statistics of the Jarque-Bera test for non-normality ([Jarque & Bera, 1980](#)) (JB) and of the Ljung-Box test for autocorrelation ([Box & Pierce, 1970](#); [Ljung & Box, 1978](#)) (Q(1) corresponds to a lag order of 1 and Q(5) lag order of 5). The null hypothesis of the Jarque-Bera is the skewness being 0 and the kurtosis being 3, and the null hypothesis of the Ljung Box test is that the residuals are serial uncorrelated when a fixed number of lags are included.

Geometric growth								
		Mean	Std	Skew	Kurt	JB	Q(1)	Q(5)
LAM	Emissions	0.036	1.010	-0.145	-0.807	1.194	0.022	1.711
	GDP	0.001	1.000	-0.415	0.283	1.826	0.265	1.627
REF	Emissions	0.091	1.014	-0.044	2.364	0.480	0.736	9.032
	GDP	0.014	1.000	-0.225	1.879	1.701	6.184*	9.108
OECD	Emissions	-0.034	1.009	-0.055	2.136	1.517	0.169	3.757
	GDP	0.000	1.000	0.565	4.075	4.862	1.114	8.146
ASIA	Emissions	0.040	1.009	0.174	3.277	0.397	0.192	2.569
	GDP	0.005	1.001	-0.287	2.973	0.659	4.722*	6.078
MAF	Emissions	0.085	1.007	-0.291	2.980	0.680	0.040	5.063
	GDP	0.011	1.001	0.337	3.448	1.309	5.531	6.663
WORLD	Emissions	0.008	1.011	-0.108	3.128	0.127	0.001	4.862
	GDP	0.005	1.000	0.478	3.080	1.838	10.071**	14.932*

D.4 Projections

Figure D.1: Comparison of the CO₂ emissions projected from the E3S2-g model plus carbon capture and storage (CCS) and from SSP 1.9 W m⁻². Confidence bands are pointwise at the 90% level.

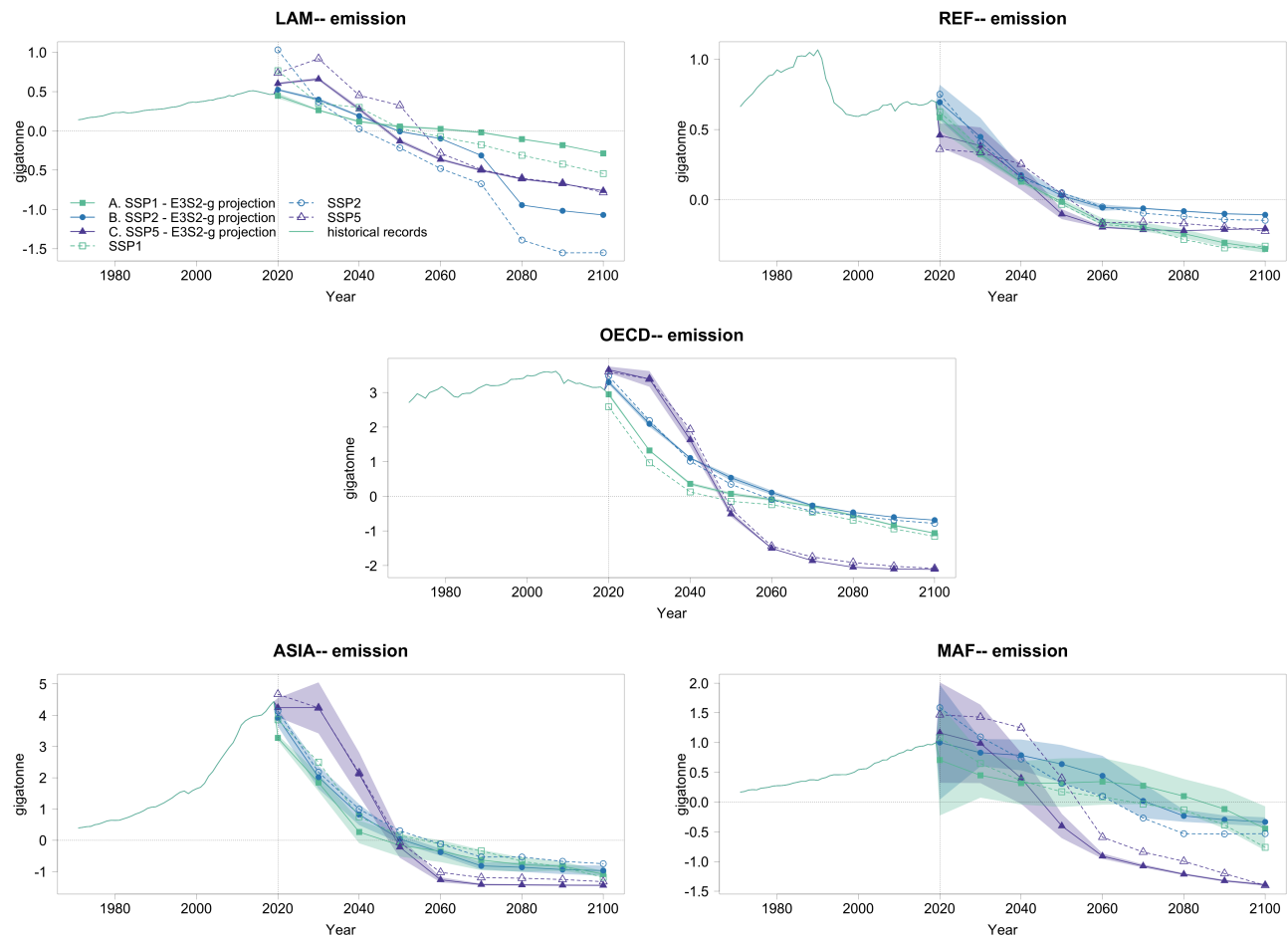


Figure D.2: Comparison of GDP projected by the E3S2-g model and SSP 1.9 W m⁻². Confidence bands are pointwise at the 90% level.

